BOREAS An international journal of Quaternary research

Defining the maximum extent of the Laurentide Ice Sheet in Home Bay (eastern Arctic Canada) during the Last Glacial episode

YAN LÉVESQUE, GUILLAUME ST-ONGE, PATRICK LAJEUNESSE, PIERRE-ARNAUD DESIAGE AND ETIENNE BROUARD

BOREAS

Lévesque, Y., St-Onge, G., Lajeunesse, P., Desiage, P.-A. & Brouard, E.: Defining the maximum extent of the Laurentide Ice Sheet in Home Bay (eastern Arctic Canada) during the Last Glacial episode. *Boreas*. https://doi.org/10.1111/bor.12415. ISSN 0300-9483.

Three sediment cores recovered on the lower slope of the continental shelf in western Baffin Bay (Arctic Canada) as well as swath bathymetry and subbottom profiler data collected on the shelf and slope of the region were analysed to investigate whether the Laurentide Ice Sheet (LIS) reached the shelf edge offshore Home Bay during the Last Glacial Maximum (LGM). Physical, sedimentological and palaeomagnetic analyses of the cores were also used to constrain the chronostratigraphy of upper sedimentary facies of the Home Bay trough-mouth fan (TMF). Seven lithofacies were identified in the cores and reveal that the sediments recorded a genuine geomagnetic signal and that the cores span the last 40 ka. In the Home Bay Trough, sets of elongated ridges are discernible on swath bathymetry imagery and are interpreted as mega-scale glacial lineations (MSGLs) resulting from an ice stream eroding the trough and delivering glacigenic sediments to the TMF. The geomorphology of the TMF, combined with the sedimentary records and the chronostratigraphy, indicates that a series of debris flows and turbidity currents were generated between 35 and 15 ka BP. These results indicate that the LIS margin extended near the shelf edge during the LGM and allow us to propose a new maximum extent of the LIS during the Last Glacial episode.

Yan Lévesque (e-mail: yan.levesque@uqar.ca), Guillaume St-Onge and Pierre-Arnaud Desiage, Institut des sciences de la mer de Rimouski (ISMER) Canada Research Chair in Marine Geology Université du Québec à Rimouski and GEOTOP, 310 allée des Ursulines, Rimouski, QC G5L 3A1, Canada; Patrick Lajeunesse, Département de Géographie, Université Laval, Québec, QC G1V 0A6, Canada; Etienne Brouard, Département des Sciences de la Terre et de l'atmosphère Université du Québec à Montréal, Montréal, QC H3C 3P8, Canada; received 12th January 2019, accepted 9th September 2019.

The Laurentide Ice Sheet (LIS) covered most of North America during the last glaciation and the eastern margin of Baffin Island, in the eastern Canadian Arctic, has been shaped by its phases of advance and retreat (Dyke & Prest 1987; Dyke 2004). Therefore, Baffin Bay, located between Baffin Island and Greenland, forms a unique setting capturing sediments related to the pulses of ice-sheet margins on the surrounding continental shelves (e.g. Simon *et al.* 2012, 2014, 2016; Brouard & Lajeunesse 2017; Jenner *et al.* 2018). Recent studies have suggested that the LIS margin extended on the north-eastern Baffin Island shelf during the Last Glacial Maximum (LGM) and reached the shelf edge (Fig. 1A, B; Li *et al.* 2011; Brouard & Lajeunesse 2017; Jenner *et al.* 2018). These studies contrast with the generally accepted LIS extent and chronologies, which portray the LIS as only extending a few kilometres seaward of the mouth of the fiords (Briner *et al.* 2005, 2006a, b). According to Dyke *et al.* (2002) ice only began to recede from its maximum position (e.g. fiord mouths) around 13–12 ka BP.

Ice-sheet dynamics near a shelf edge can generate considerable temporal and spatial variability in the depositional processes of glacigenic sediments onto the continental slope and in ocean basins (Laberg & Vorren 1995; King *et al.* 1998; Vorren *et al.* 1998; Nygård *et al.* 2002). A range of sedimentary processes have been described and include glacigenic debris flows (GDFs) and turbidity currents, which flow through canyons and gullies, and can accumulate tens to hundreds of kilometres down-slope on submarine deep sea fans (e.g. TMFs; Laberg & Vorren 1995; Vorren *et al.* 1998; Ó Cofaigh *et al.* 2003; De Blasio *et al.* 2004; Tripsanas & Piper 2008). TMFs are generally composed of stacked glacigenic debrites that in some cases alternate laterally with turbidites also of glacial origin; they can therefore be used to identify periods of glacial activity at the shelf edge (e.g. Laberg & Vorren 1995; Vorren *et al.* 1998; Tripsanas & Piper 2008). Establishing the temporal evolution setting of the sediment accumulation within a TMF can, however, be highly challenging due to chronostratigraphical limitations. Indeed, datable material such as biogenic carbonates are scarce and/or not well preserved in the Canadian Arctic, especially in Baffin Bay (de Vernal *et al.* 1987, 1992; Ledu *et al.* 2008; McKay *et al.* 2008; Simon *et al.* 2012). To circumvent these issues, palaeomagnetism combined with radiocarbon dating can provide an age control on the glacigenic triggering events (Stoner & St-Onge 2007; St-Onge & Stoner 2011). Sediment cores taken offshore of high-latitude continental margins are particularly well suited for high-resolution Quaternary palaeoenvironmental reconstructions and can provide continuous and reliable records of variations in the geomagnetic field (e.g. Andrews & Jennings 1990; Snowball & Sandgren 2002; Snowball & Muscheler 2007; Barletta *et al.* 2008).

Here, we present a palaeomagnetic sequence of the relative palaeointensity from the continental margin of

DOI 10.1111/bor.12415

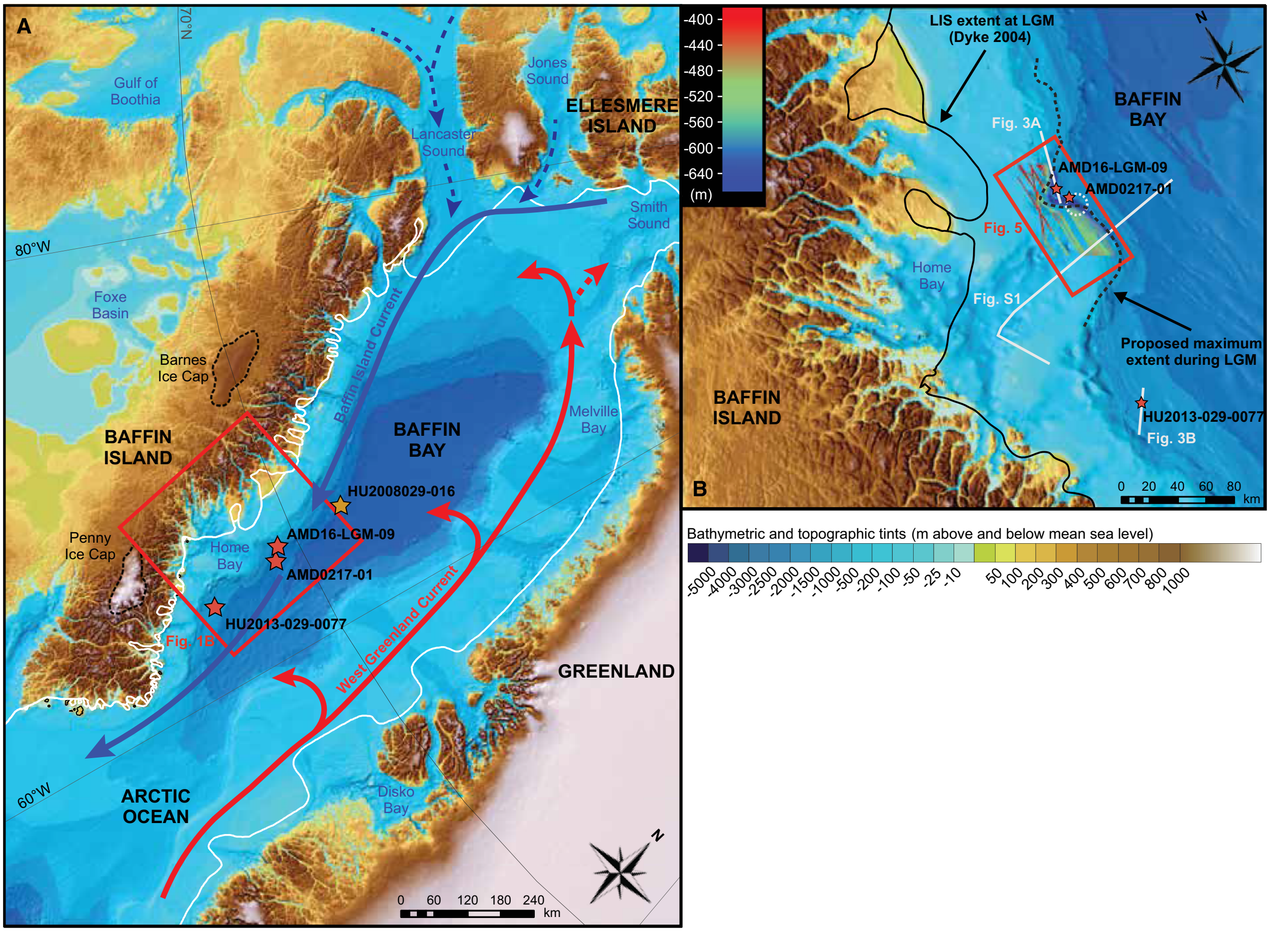

Fig. 1. A. Topographic and bathymetric map of the Baffin Bay area (Jakobsson *et al.* 2012). The red stars show the locations of the sampling sites from this study: cores HU2013-029-0077 (77PC), AMD0217-01 PC and TWC (1Comp) and AMD16-LGM-09CASQ (9CASQ). The yellow star shows the location of core HU2008-029-016PC from Simon *et al.* (2012). The simplified ocean circulation is represented by the red arrows to illustrate the warm West Greenland current and by the blue arrows to represent the cold Baffin Island current. The white lines represent the ice margin at 16.5 cal. ka of the Laurentian (LIS), Innuitian (IIS) and Greenland (GIS) ice sheets according to Dyke (2004). The red square is the focus of Fig. 1B. B. The dashed black line represents the maximum extent proposed in this study. The solid black line represents the maximum extent according to Dyke (2004). The red stars represent the sampling sites of cores 77PC, 9CASQ and 1Comp. Solid white lines refer to the locations of the seismic profiles shown in Figs 3A, B and S1. The white dashed circle refers to Fig. 4. The red rectangle is the location of the multibeam image of Fig. 5A and B. See text for details.

Baffin Island and compare this sequence to one palaeomagnetic record from Baffin Bay (Simon *et al.* 2012) and two others palaeomagnetic stacks from the North Atlantic and Mediterranean Sea/Somalian Basin (Meynadier *et al.* 1992; Laj *et al.* 2000) to obtain a time frame for the cores collected from Home Bay TMF, in order to determine if the LIS reached the shelf edge during the LGM. In addition, we use swath bathymetry and subbottom profiler data to identify landforms and deposits left by the LIS on the Home Bay cross-shelf trough and fan.

Regional setting

Baffin Bay forms a narrow (450 km wide) oceanic basin located between the Canadian Arctic Archipelago and Greenland that is characterized by an anticlockwise ocean circulation (West Greenland and Baffin Island currents; Fig. 1A) and by partial sea ice cover during most of the year (Tang *et al.* 2004). Archaean and Palaeoproterozoic cratons form the main geological units on either side of Baffin Bay, and are overlain by a succession of Palaeozoic rocks dominated by shallow carbonates such as dolostones and limestones (Aksu & Piper 1987; Hiscott *et al.* 1989; Simon *et al.* 2012; Stanley & Luczaj 2015).

During the LGM, Baffin Bay was surrounded by three major ice sheets that flowed into it: the Greenland Ice Sheet (GIS), the Laurentian Ice Sheet (LIS) and the Innuitian Ice Sheet (IIS) (Dyke & Prest 1987; Dyke *et al.* 2002; Stokes 2017). The LIS extended across Baffin Island and possibly covered much of the fiords and the continental shelf (Briner *et al.* 2006a, b; Funder *et al.* 2011). Quaternary deposits from Baffin Bay, mainly debris flows and turbidites, also suggest that the LIS may have reached the Baffin Island continental shelf during the LGM (Aksu & Piper 1987; Hiscott & Aksu 1994; Praeg *et al.* 2006). These turbidites and debrites relate to meltwater processes that periodically incised canyons and submarine valleys on TMFs (e.g. Tripsanas & Piper 2008; Li *et al.* 2012). Therefore, they record periods of ice occupying the troughs. Basal diamictons are often observed in sediment cores collected on the NE Baffin slope near the mouths of TMFs (Table 1, Fig. 2). They usually represent GDFs that were triggered by glacial advance during the LGM (Jenner *et al.* 2018). Deglaciation of the LIS in Baffin Bay is thought to have begun around 16–15 cal. ka BP, but only beginning around 13–12 cal. ka BP in Home Bay (Dyke & Prest 1987; Dyke *et al.* 2002; Dyke 2004).

Material and methods

Sediment cores

Two piston cores and one large square gravity core (CASQ) were collected with their companion trigger weight cores (TWC) and associated box cores (BC) in central Baffin Bay in 2016 and 2017. Cores AMD16-LGM-09 and AMD0217-01, hereinafter referred as cores 9CASQ and 1Comp, were collected aboard the CCGS Amundsen from the Home Bay TMF; core HU2013-029-0077 (hereinafter referred as 77PC) was collected in 2013 aboard the CCGS 'Hudson' during cruise 2013029 with the purpose of serving as a chronostratigraphical reference core (Table 1, Fig. 1; Campbell 2014).

Seismo-stratigraphy and swath bathymetry

High-resolution swath bathymetry data were acquired using a hull-mounted Kongsberg EM-302 (30 kHz) echo-sounder. High-resolution acoustic subbottom data were collected with a Knudsen 3.5 kHz Chirp system and analysed using The Kingdom Suite software (IHS). Subbottom profiles were analysed onboard in order to identify areas of Quaternary sedimentary sequences in which mass movements and/or sediment perturbations were present inside the TMF (i.e. the coring sites). The geomorphology of the Home Bay area was mapped by the interpretation of the swath bathymetric data, which were processed using the CARIS HIPS and SIPS software and then visualized with the QPS Fledermaus software. Finally, airgun seismic reflection data (Line 76029_AG_280_1730) were acquired through the public database of the National Resources Canada Marine Data Holdings. The airgun data were used to investigate the sedimentary architecture of the cross-shelf trough in search of potential grounding-zone wedges (GZW) in the area.

Table 1. Coordinates and properties of the coring sites.

Core	Latitude (°N)	Longitude (°W)	Location	Water depth (m)	Length (cm)
HU2013-029-0077	69.31	63.79	Slope	1153	597
AMD16-LGM-09 CASQ	68.28	64.56	Slope (TMF)	1220	554
AMD0217-01 PC/TWC	69.24	64.43	Slope (TMF)	1076	350/152
Composite	69.24	64.43	Slope (TMF)	1076	380

Physical and geochemical properties

To define the stratigraphy and sedimentary facies, sections of core 9CASQ were passed through a computerized axial tomography scanner (CAT-Scan) at the Institut national de la recherche scientifique, Centre Eau Terre Environnement (INRS-ETE) in Québec City to characterize the sedimentary facies and sediment structures (St-Onge *et al.* 2007). Similarly, the sections of core 1Comp were scanned with a GEOTEK XCT digital X-ray system at ISMER (Fig. 2). Whole cores were then analysed using a GEOTEK Multi Sensor Core Logger (MSCL) at 1-cm intervals to measure the low-field volumetric magnetic susceptibility (k_{LF}) and the wet bulk density using gamma-ray attenuation; then, the core was split, described and photographed. Diffuse spectral reflectance was then acquired with an online Minolta CM-2600d spectrophotometer at 0.5-cm intervals, while the concentrations of minor and major chemical elements (calcium (Ca), strontium (Sr), iron (Fe), rubidium (Rb), amongst others) were determined by X-ray fluorescence (XRF) spectrometry for the same intervals using an Olympus Innov-X Handheld Delta XRF analyser integrated to the MSCL. The grain-size analysis was performed at 10-cm intervals on bulk sediment samples at ISMER using a Beckman Coulter™ LS13320 laser diffraction grain-size analyser, as well as at a higher resolution in specific facies such as in turbidites. Prior to analyses, samples were sieved at 2 mm. Apart from a few intervals with a few pebbles, no material larger than 2 mm was recovered. Therefore, the size fraction larger than 2 mm has been excluded from the grain-size metrics.

Palaeomagnetic analysis

Palaeomagnetic data were measured at 1-cm intervals on u-channel samples (2×2×150 cm) using a 2G Enterprises™ cryogenic magnetometer at ISMER for chronostratigraphical purposes and to identify possible rapidly deposited layers such as turbidites and debrites, which are characterized by low-quality palaeomagnetic data and shallow inclinations (e.g. St-Onge *et al.* 2004; Tanty

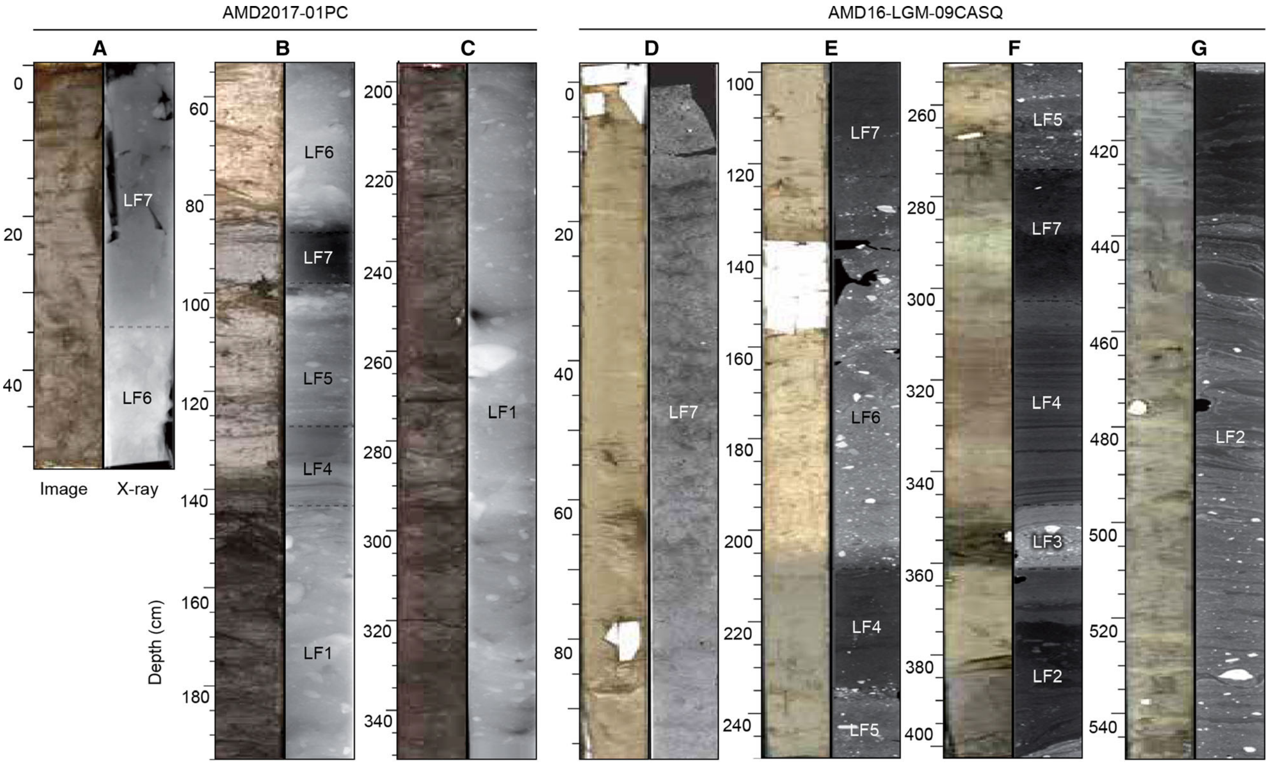

Fig. 2. X-radiographs and high-resolution photography of representative lithofacies from sediment cores of Home Bay TMF: AMD0217-01 PC and AMD16-LGM-09CASQ(9CASQ). Massive, matrix-supported diamicton facies. Complex diamicton (LF1); Laminated mud rich in IRD (LF2); Silt and sand turbidite (LF3); Laminated mud (LF4); Homogenous mud with IRD (LF5); Carbonate-rich bed with IRD (LF6); Homogenous mud without IRD (LF7). The grey dashed lines define facies changes. See Fig. 7 for facies identification legend and sediment characteristics. Add 30 cm to obtain the real depths of 1Comp.

et al. 2016). The measurements performed were as follows: natural remanent magnetization (NRM), anhysteretic remanent magnetization (ARM), isothermal remanent magnetization (IRM) and saturation isothermal magnetization (SIRM). Due to the finite spatial resolution of the pick-up coils that integrates measurements over ~7–8 cm (Philippe *et al.* 2018), some smoothing occurred. To eliminate the edge effect associated with this response function, the data from the first and last 4 cm of each u-channel were excluded.

The NRM was measured and then progressively demagnetized using stepwise alternating field demagnetization (AF) at peak fields from 0 to 75 mT at 5-mT increments. Directions (inclination and declination) of the characteristic remanent magnetization (ChRM) were calculated using the Excel spreadsheet developed by Mazaud (2005) with AF demagnetization steps from 10 to 60 mT (11 steps) for the three cores. This method also provides maximum angular deviation (MAD) values, which are indicative of high-quality directional data for Quaternary palaeomagnetic studies if the MAD is lower than 5° (Stoner & St-Onge 2007). Using this spreadsheet, the median destructive field (MDF) of the NRM is also calculated. The MDF represents the required demagnetization field necessary to reduce the initial magnetic remanence by half of its initial intensity. The MDF is an indicator of magnetic mineralogy, reflects the mean coercivity state of the magnetic grain assemblage and depends on both the grain size and the mineralogy (e.g. Stoner & St-Onge 2007; Barletta *et al.* 2010). The ARM was then induced using a 100 mT AF with a 0.05 mT direct current (DC) biasing field. The ARM was then demagnetized and measured from 0 to 75 mT at every 5 mT. Two IRMs were imparted with a DC field of 0.3 T (IRM) and 0.95 T (SIRM) using a 2G Enterprises pulse magnetizer. Each IRM was measured from 0 to 75 mT at 5-mT demagnetization step increments; the steps used in the SIRM were 0, 10, 30, 50 and 70 mT.

To define the magnetic mineralogy, hysteresis measurements were performed at 10-cm intervals on a small quantity of sediment from the three cores using a Princeton Measurement Corporation MicroMag 2900 alternating gradient force magnetometer (AGM). The saturation magnetization (Ms), the coercive force (Hc), the saturation remanence (Mrs) and the coercivity of remanence (Hcr) were extracted from the hysteresis data to characterize the magnetic mineralogy and grain size (Day *et al.* 1977).

Radiocarbon dating

To develop the chronology of the cores, ^{14}C ages were obtained by accelerator mass spectrometry (AMS) on six samples from mixed planktonic and benthic foraminifera and one sample derived from *Neogloboquadrina pachyderma* shells (Table 2) at the Laboratoire des sciences du climat et de l'environnement (LSCE), Gif-sur-Yvette, France (cores 9CASQ and 1Comp). The conventional ages were then calibrated using the CALIB 7.1 online calibration software (Stuiver *et al.* 2017) and the MARINE13 calibration curve (Reimer *et al.* 2013) with a regional reservoir correction Δ*R* of 220±20 years (Coulthard *et al.* 2010). Of the six samples that were analysed, only the results of sample ECHo 2559 could not be validated, as only 1 μg of carbon was detected.

Results

Sea-floor morphology and stratigraphical framework

Subbottom profiles. – The acoustic subbottom profiles (3.5 kHz) from the sampling location of core 9CASQ show high-amplitude parallel acoustic reflections at the middle of the core (between 362 and 125 cm) where a turbidite and alternating mud and ice-rafted debris (IRD) layers are observed. These units are topped by an acoustically transparent unit associated with postglacial hemipelagic sediments (Fig. 3A). However, given the loss of the signal at the base of the core (between 552 and 362 cm), the seismic profile in Fig. 3A does not reflect the stratigraphy at the base. The seismic profile of core 77PC is modified from Campbell & Bennett (2014) and is characterized by high-amplitude parallel reflections in the basal part of the core and transparent acoustic facies associated with the hemipelagic sediments in the upper part of the core (Fig. 3B; Campbell & Bennett 2014). For core 1Comp, the sequence is characterized by a high-amplitude reflection that can be associated with the debrite observed at the base of the core, whereas the uppermost acoustically transparent unit is interpreted as postglacial hemipelagic sediments (Fig. 4). The available data within the cross-shelf trough, including the airgun profile (Fig. S1), do not show any seismic unit that could be interpreted as a GZW.

Swath bathymetry. – Glacigenic landforms associated with the presence of the LIS and/or icebergs drifting offshore were identified and mapped using the swath bathymetry imagery. Linear, curvilinear, and almost circular depressions with a general N–S orientation, occur at the eastern end of the trough. These are interpreted as the product of iceberg keels eroding the sea floor (Figs 5A, B, S2; Brouard & Lajeunesse 2019a). Sets of other erosional landforms aligned parallel to the trough axis (W–E) are also observed in the Home Bay Trough. Three distinct landforms can be interpreted within the trough: (i) large ridges that are similar in terms of width (km) to subglacial medial moraines in other Baffin Island troughs (Brouard & Lajeunesse 2017); (ii) smaller-scale longitudinal ridges that have morphologies similar to mega-scale glacial lineations (MSGLs; Clark 1993; Stokes & Clark 2002); and (iii) curvilinear depressions that are interpreted as iceberg scours (Fig. 5B). The seaward end of the cross-shelf trough is characterized by a series of parallel gullies, some of which extend downslope to form turbidity channels with distinctive levees (Figs 5A, S2, S6). Such channels are generally eroded by underflows or currents transporting sediment downslope and have been reported on other high-latitude shelves and in fiords (Syvitski & Shaw 1995; Syvitski *et al.* 2012; Dowdeswell & Vásquez 2013; Brouard & Lajeunesse 2019b).

Lithofacies

The classification of these facies was determined from CAT-scan images, physical and magnetic properties, as well as previous studies from Baffin Bay (Andrews 1985; Tripsanas & Piper 2008; Simon *et al.* 2012; Ó Cofaigh *et al.* 2013; Jackson *et al.* 2017; Jenner *et al.* 2018). Photography and CAT-scan images reveal a highly variable lithology across the cores (Figs 2, 7). Overall, seven lithofacies were identified in the two cores from the TMF (1Comp and 9CASQ; Figs 6, 7). Lithofacies 1 (LF1) is defined as a massive, matrix-supported diamicton facies with very dense, black, and coarse-grained

Table 2. Radiocarbon ages from cores HU2013-029-0077 (77PC), AMD0217-01 PC (01-PC) and AMD16-LGM-09CASQ (9CASQ). Radiocarbon ages were calibrated using CALIB version 7.1 (Stuiver *et al.* 2017) and the Marine13 calibration curve (Reimer *et al.* 2013). Radiocarbon ages from core HU2013-029-0077 are from Jenner *et al.* (2018).

Core	Depth (cm)	Material	Conventional age (a BP)	Calibrated age (cal. a BP)	Lab. number
77PC	142	Mixed benthic foraminifera	10 550±40	11 327	OS-117723
	205	Mixed planktonic foraminifera	12 750±55	14 013	OS-118359
	644 (core catcher)	*Neogloboquadrina pachyderma*	37 900±1600	41 461	OS-UCIAMS 181265
01-PC	109 (not valid)	Mixed benthic and planktonic foraminifera	10 180±1490	11 029	ECHo 2559
	135	Mixed benthic and planktonic foraminifera	12 820±60	14 088	ECHo 2558
9CASQ	465	Mixed benthic and planktonic foraminifera	35 160±760	39 024	ECHo 2458

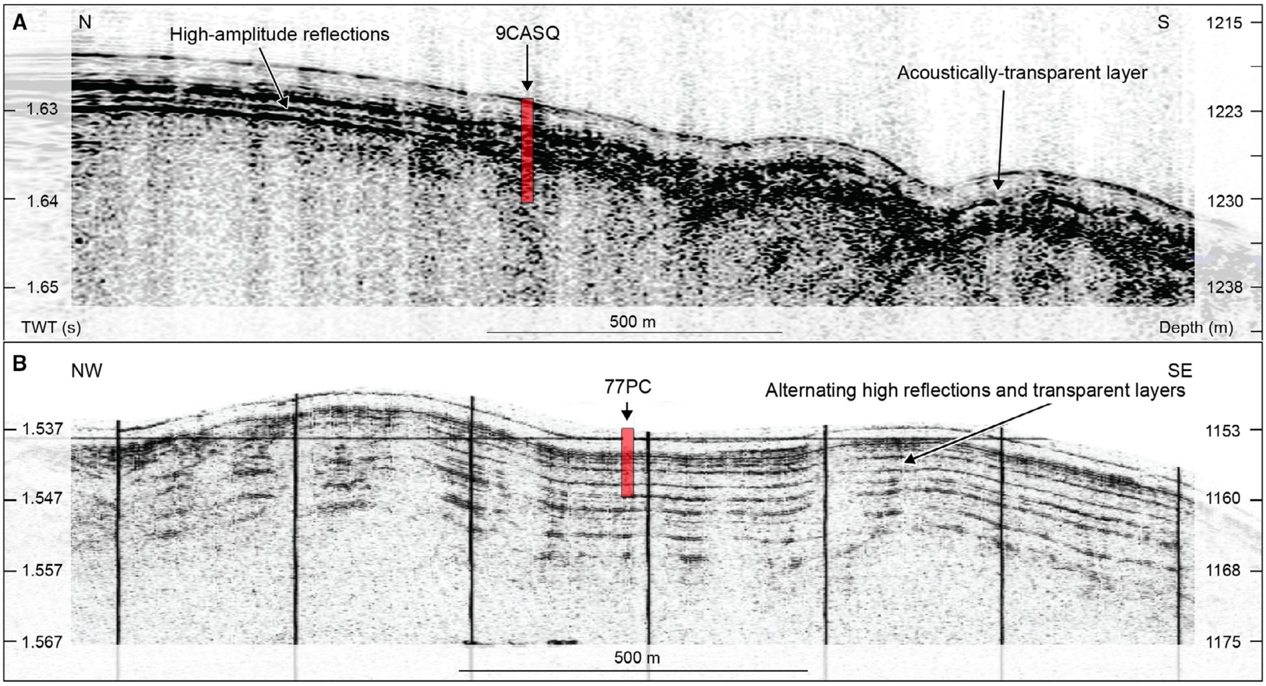

Fig. 3. A. Acoustic (Chirp) subbottom profile over core 9CASQ site and located at the lower end of the continental slope of the Home Bay TMF near the abyssal plain. B. Huntec subbottom profile collected in 1978, showing the thick acoustically stratified interval of core 77PC located on the continental slope of Home Bay. The estimated core depths are indicated with red marks. Fig. 3B is modified from Campbell & Bennett (2014). The acoustically transparent layers represent postglacial sediments and the high-amplitude reflections represent alternation of mud, IRD layers and turbidite.

sediment. It is mixed with a fine-grained matrix and has a sharp upper contact. This facies contains a concentration of granules, pebbles and cobbles, which are angular to subrounded in shape. Lithofacies 2 (LF2) is defined as a laminated dark grey to dark greyish-brown silty mud, rich in IRD, with an unrhythmic succession of stratified pebbly mud. The concentrated pebbles often deform the laminae and contacts range from diffuse to sharp (Fig. 2). Lithofacies 3 (LF3) is defined as dense, very dark grey silts and sands with clasts. Facies LF3 is

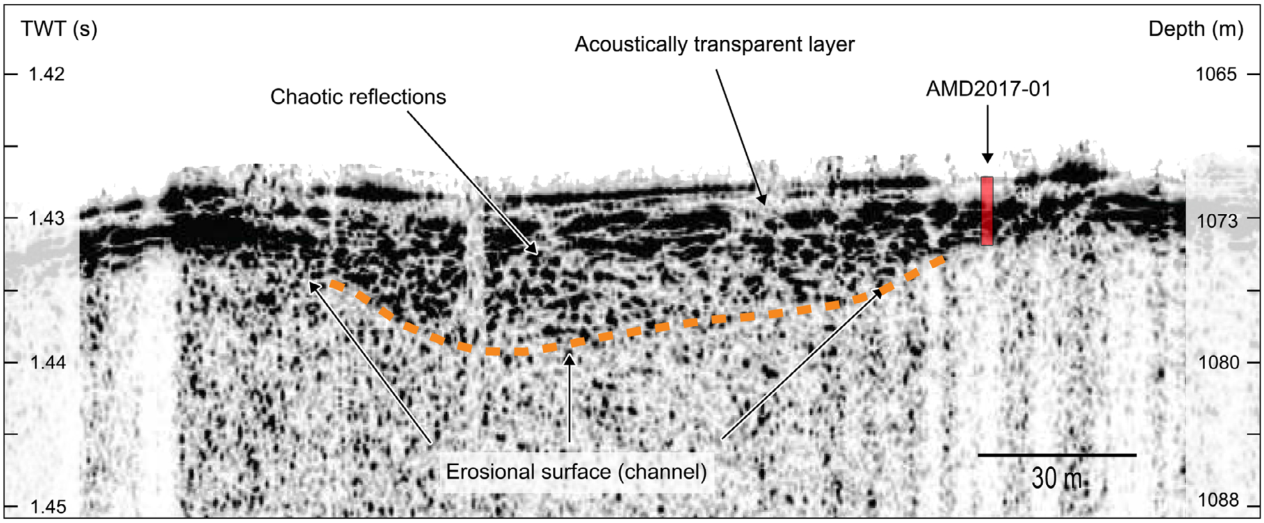

Fig. 4. Acoustic (Chirp) subbottom profile over core AMD0217-01 PC (1Comp) site located at the lower end of the continental slope of Home Bay. The orange dashed line delimits a buried debris flow channel just aside of the core. The chaotic character of the infill on the profile is attributed to debris flow deposits. This channel is composed of a series of stacked debris flows that accumulated inside the TMF. The estimated core depths (~4 m) are indicated with the red mark.

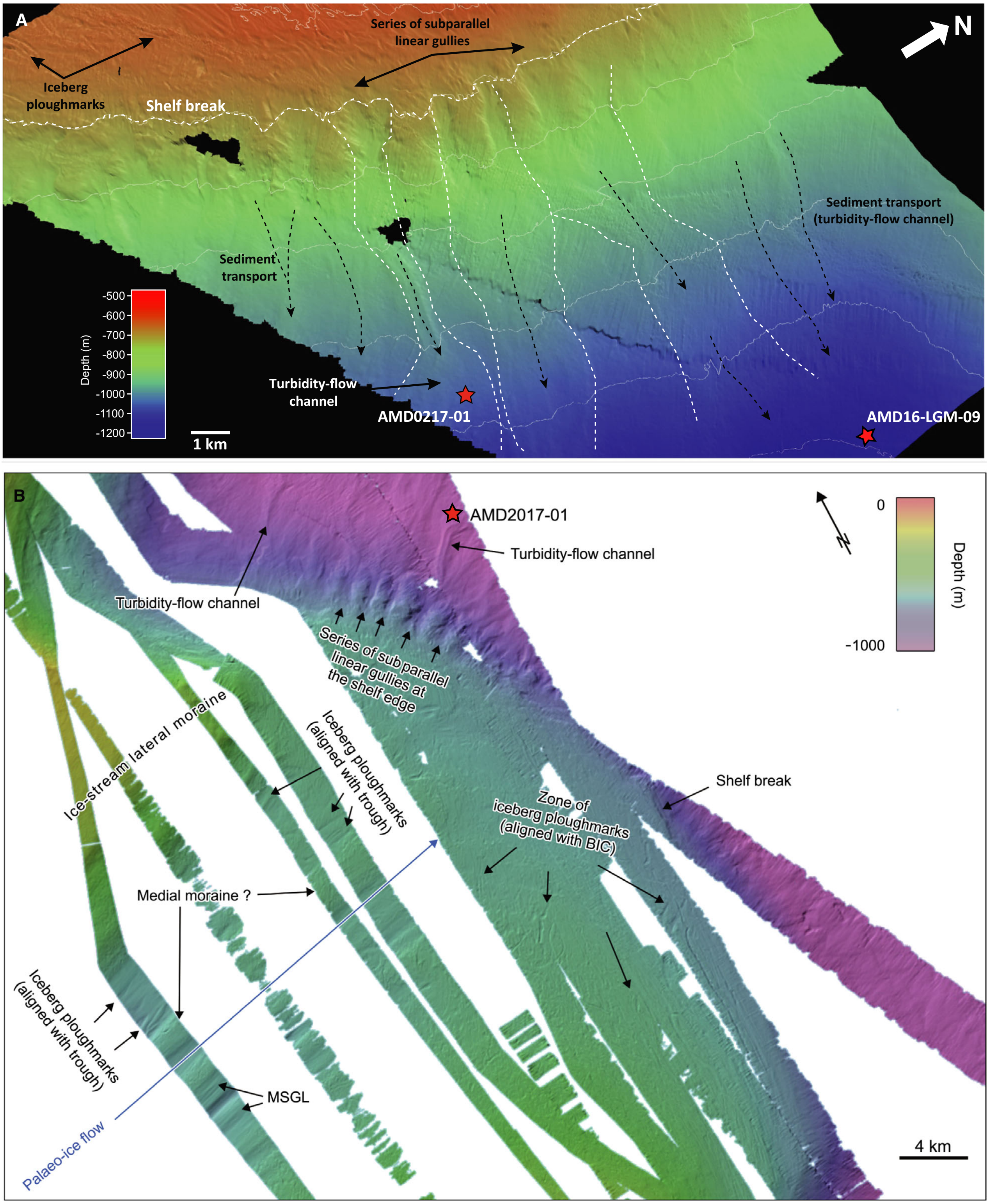

Fig. 5. A. Angled view of the submarine morphology of the TMF showing gullies and iceberg ploughmarks. The white dashed lines correspond to the limit of three turbidity channels upstream of cores 9CASQ and 1Comp (AMD0217-01). The black dashed lines represent sediment transport pathways. B. Swath bathymetry imagery showing elongated landforms interpreted as mega-scale glacial lineations (MSGLs) and iceberg ploughmarks on the shelf. See text for details.

composed of coarse-based fining upward laminated mud with normal grading (Fig. 8). The upper contact of this layer is also visible, as shown by the contrast between the finer sediment and the background sediments immediately above (Figs 6, 8; St-Onge *et al.* 2004; Bourget *et al.* 2011; Pouderoux *et al.* 2012). Lithofacies 4 (LF4) is defined as a laminated dark greyish-brown rhythmic succession of clay and silt laminae. The laminae and contacts range from diffuse to very sharp and do not contain IRD or bioturbation. Lithofacies 5 (LF5) is defined as a massive homogenous dark greyish-brown silty mud with IRD. No apparent structures are observed. The distribution of pebbles within LF5 ranges from dispersed to concentrated and the contacts range from diffuse to gradual. Lithofacies 6 (LF6) is defined as a carbonate-rich light olive brown sandy and pebbly mud with IRD. Finally, lithofacies 7 (LF7) is defined as a massive and homogenous bioturbated greyish to brownish mud without IRD. Apart from traces of bioturbation such as well-defined burrows, no apparent structures are observed in this lithofacies (Fig. 2).

Interpretation of lithofacies

LF1 exhibit characteristics (massive, matrix-supported diamicton facies) that are similar to GDFs triggered near an ice-sheet margin and that have been described at the margin of other deglaciated shelves (King *et al.* 1998; Ó Cofaigh *et al.* 2013). The IRD-rich, silty mud of the LF2 facies suggests that it was probably deposited during episodes of warming leading to sea ice cover break-ups, which enable icebergs to drift along currents (Dowdeswell *et al.* 2000). However, the laminated character of LF2 also suggests other possible processes for deposition; the laminations could result from turbidity current activity and/or turbid meltwater plumes originating from glacial ice on the shelf. These laminations would reflect the evolution in time of meltwater discharge from proximal tidewater glaciers (Cowan & Powell 1990; Andrews *et al.* 1991; Dowdeswell & Cromack 1991; Jennings 1993; Dowdeswell *et al.* 2000; Jenner *et al.* 2018). This assumption is supported by the fact that during winter or a long phase of climate cooling, ice covers all of Baffin Bay and traps icebergs, suppressing their drift offshore. In this case, meltwater discharge will be dominant if there is no delivery of coarser debris. Cowan *et al.* (1997) suggested the opposite and proposed punctuated IRD deposition occurs in winter and turbid meltwater deposition, dominated by turbidity currents and suspension deposits, occurs in summer. One way or the other, the fine-grained laminated glaciomarine sediments are usually not regarded as typical of iceberg-dominated areas, but sometimes they can vary rhythmically with IRD and rapidly deposited layers (Domack 1990; Dowdeswell *et al.* 2000). Overall, both processes (IRD and turbidity current deposition) probably reflect punctuated IRD deposition during winters and turbid meltwater deposition, dominated by turbidity currents and suspension deposits, during summers (Cowan *et al.* 1997). A similar layer in core 9CASQ represents a glaciomarine environment. Suspension deposit sedimentation during periods of continuous sea ice cover probably generated the mud of this unit. The hypothesis of multiyear sea ice cover of the core sites is reinforced by the scarcity of foraminifera, as continuous sea ice cover suppresses biological activity (Syvitski 1989; Dowdeswell *et al.* 2000).

The coarse-grained laminated mud at the base of LF3 and its normal grading is suggestive of a silty and sandy turbidite. Core 9CASQ was collected at 1220 m water depth and contains a LF3 Layer (Figs 6, 8). As the Baffin Island Current (BIC) is particularly strong at 1000–1200 water depth on the Baffin Bay Slope (Dunlap & Tang 2006), they can trigger low-density muddy turbidity currents. As a result of this bottom current activity, LF3 facies can be interpreted as a turbidite (Dunlap & Tang 2006; Roger *et al.* 2013; Jenner *et al.* 2018).

Rhythmic successions of clay and silt laminae with diffuse contacts and without IRD and bioturbation in LF4 can be deposited through various processes in northern environments, such as the deposition by meltwater plumes (Hesse *et al.* 1997), as mud turbidites seaward of glacial troughs (Roger *et al.* 2013) and as subglacial outbursts of turbid meltwaters (Lucchi *et al.* 2013). In cores 9CASQ and 1Comp, this facies mostly overlies a debrite or turbidite. We therefore associate it with muddy density flows and meltwater plumes emanating from glacial discharge during ice retreat.

The massive and homogenous character of LF5 mud indicates a low-energy environment that probably reflects the absence of glacial activity near the core site. The frequent IRD of LF5 relate to drifting icebergs and suggests that a significant portion of Home Bay was ice-free at this time.

The carbonate-rich sandy and pebbly mud with IRD of LF6 is similar to ice-rafted, carbonate-rich sediments observed all around Baffin Bay (Andrews *et al.* 1998, 2009; Jackson *et al.* 2017). These layers, named Baffin Bay Detrital Carbonate layers (e.g. Andrews *et al.* 1998; Simon *et al.* 2014) are associated with episodes of high iceberg activity originating from NW Baffin Bay (Aksu & Piper 1987) and have been dated to 10.5–12 (BBDC0) and 13.7–15 cal. ka BP (BBDC1; Simon *et al.* 2014). Aksu & Piper (1987) suggested that northwestern Baffin Bay, Devon and Ellesmere Islands and northwestern Greenland are the source of the lower Palaeozoic limestones and dolomites observed in sediments transported as IRD to southern Baffin Bay. In contrast with the previous facies, which were rich in IRD, LF7 contains massive and homogenous bioturbated mud without IRD in the uppermost part of the core and reflects hemipelagic sedimentation in a postglacial environment similarly to other uppermost parts of cores recovered in Baffin Bay (e.g. Dowdeswell *et al.* 2008; Ó Cofaigh *et al.* 2013).

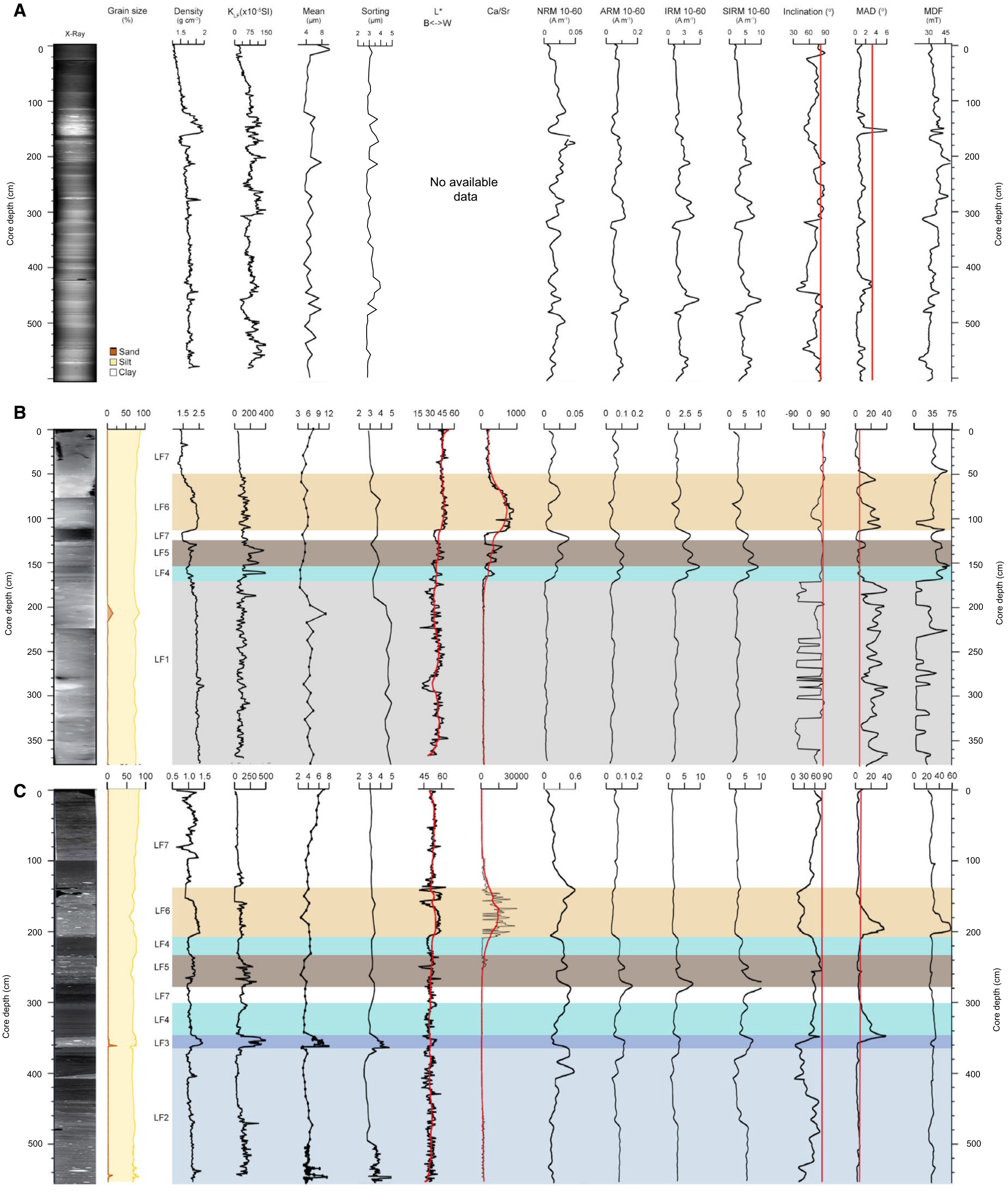

Fig. 6. High-resolution physical, geochemical and magnetic properties of cores 77PC (A), 1Comp (B) and 9CASQ (C). See Fig. 7 for more details on facies identification. The vertical red lines delineate the MAD value of 5° and the expected inclination, respectively, according to a geocentric axial dipole (I_{GAD}) at the coring site. Sediments were sieved at 2 mm prior to grain size analysis and no sediments coarser than 2 mm, except for occasional pebbles, were recovered. Therefore, the >2 mm size fraction has been excluded from the grain-size metrics.

Physical, stratigraphical and magnetic properties

Core 77PC. – Core 77PC is used here as a chronostratigraphical reference core; Jenner *et al.* (2018) provided a detailed description of the core together with original ages. Overall, this core is composed of laminated and bioturbated mud, wavy silty laminae and detrital carbonate layers but contains no rapidly

X-ray	Image	Facies	Sedimentary	
			Structures	Processes
055 cm  060 cm		Homogenous mud without IRD (LF7)	Bioturbated greyish to brownish mud without IRD. No apparent structure are observed.	Hemipelagic sedimentation (postglacial).
179 cm 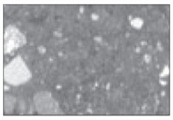 183 cm		Carbonate rich bed with IRD (LF6)	Light olive brown sandy mud and pebbly mud rich in IRD.	Hemipelagic sedimentation with frequent IRD (deglacial/postglacial).
250 cm  260 cm		Homogenous mud with IRD (LF5)	Dark greyish brown silty mud with IRD. No apparent structures are observable.	
343 cm 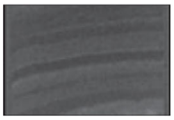 347 cm		Laminated mud (LF4)	Dark greyish brown rhythmic succession of mud and silt laminae.	Meltwater plume, turbidity current and possible bottom current influence (deglacial).
354 cm 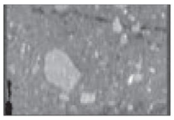 360 cm		Silt and sand turbidite (LF3)	Dense and very dark grey silt and fine sand with clast.	Turbidity current (glacial environment).
490 cm 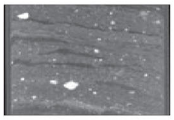 498 cm		Laminated mud rich in IRD (LF2)	Succession of dark gray to dark greyish brown silty laminated mud rich in IRD.	Meltwater plume, ice rafting and turbidity current (glacial environment).
258 cm  273 cm		Complex diamicton (LF1)	Massive, matrix-supported diamict facies. Very dense, black and coarse-grained sediment mixed with a fine-grained matrix.	Glacigenic debris flow (glacial environment).

Fig. 7. Sediment facies characteristics of cores 1Comp and 9CASQ. From left to right: X-radiographs, high-resolution photography, facies, sedimentary structures and processes along with the depositional environment.

deposited layers. The grain-size results show relatively fine material with an average of ~5 μm in the entire core (Fig. 6A). Between 161 and 117 cm, a sharp increase in the density and MAD values is observed, as well as a decrease in the inclination and NRM values. Aside from this interval, the NRM values are relatively constant (~0.02 A m^{-1}), but peaks are seen in the ARM, IRM and SIRM profiles between 310 and 270 cm, as well as between 470 and 450 cm (Fig. 6A). Nonetheless, the MAD values are lower than 5° in the entire core, indicating high-quality palaeomagnetic data except for a few intervals.

The ChRM was determined after using 5 mT demagnetization steps between 10 and 60 mT. The ChRM fluctuates around the expected inclination value for the coring site that was calculated according to the geocentric axial dipole model (I_{GAD}), denoting a well-recorded palaeomagnetic signal (Fig. 6A; Stoner & St-Onge 2007). The down-core MAD values are generally lower than 2°, indicative of a very well-defined ChRM. The MDF_{NRM} values fluctuate between 20 and 40 mT throughout the core with an average of 35 mT. Such an average indicates the presence of low coercivity minerals such as magnetite, except for a few very thin intervals where MDF values close to 50 mT are observed.

Core 1Comp. – The correlation between the density measured on the piston and the trigger weight core 01 suggests that approximately 30 cm of sediment was lost during the piston coring. This missing sediment was taken into account when constructing the composite profile (Fig. S3).

The physical and magnetic properties allow the identification of five distinct stratigraphical units (Figs 6B, 7). The base of the core extends from 381 to 175 cm and is characterized by a thick and poorly sorted layer with high

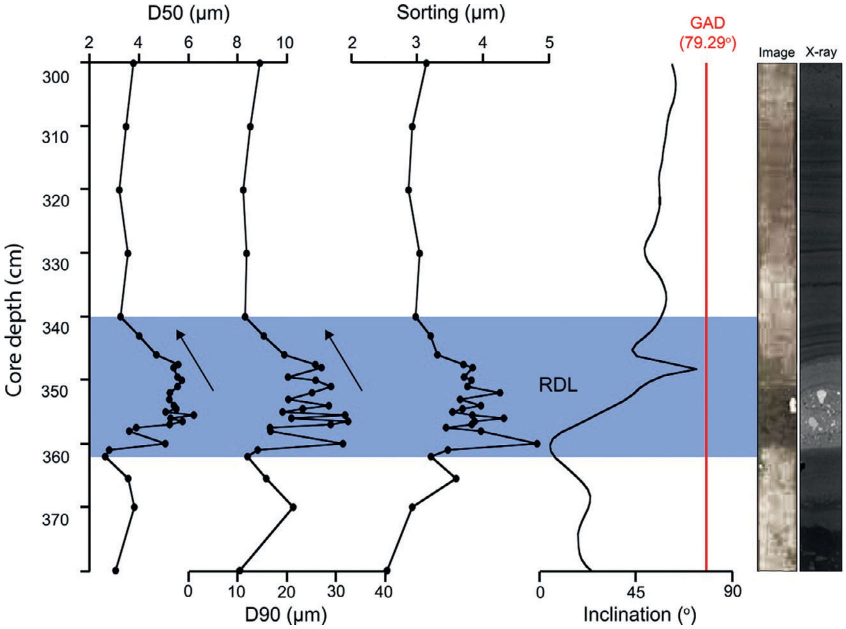

Fig. 8. Grain-size signature (D50, D90, sorting) and inclinations of LF3 in core 9CASQ sampled in the lower continental slope of Home Bay. These trends illustrate the normal grading of a turbidite. The arrows represent the grading. The >2 mm size fraction has been excluded from the grain-size metrics.

density values. This layer in core 1Comp is the LF1 facies, which is absent in cores 77PC and 9CASQ.

Overlying LF1, the LF4 layer extends from 175 to 161 cm, has low magnetic susceptibility, good sorting and a mean grain size ~3 µm. The coarse material from LF5 (161–129 cm) reflects the high values of magnetic susceptibility that peaks at approximately 400×10^{-5} SI, which is due to the presence of pebbles containing a high concentration of ferrimagnetic minerals. Unit 5 (LF5) extends from 161 to 129 cm.

Over LF4 lies a layer (117–65 cm) showing distinct peaks in Ca/Sr ratio (Fig. 6B) reflecting a high carbonate content. The Ca/Sr ratio averages approximately 100 throughout the core 1Comp, but reaches 750 at 85 cm. In addition, between 117 and 65 cm, the MAD values reach 30° at 100 cm, as well as a decrease in inclination and remanence values (NRM, ARM, IRM, SIRM; Fig. 6B). These results attest to the presence of detrital carbonate probably associated with BBDC events (Fig. 6B; e.g. Balsam *et al.* 1999; Hodell *et al.* 2008; Channell *et al.* 2012; Winsor *et al.* 2012; Simon *et al.* 2014, 2016; Jackson *et al.* 2017). LF7 tops the core from 65 to 0, but also from 129 to 117 cm.

The NRM, ARM, IRM and SIRM values are variable throughout this core (Fig. 6B). Inclination values in this core also generally fluctuate around the expected values of the GAD with MAD values below 5°, indicating high-quality palaeomagnetic data (Stoner & St-Onge 2007; Tauxe 2010). Shallower inclinations and much higher MAD values are observed between 381–175 (LF1), 161–115 and 117–65 cm (BBDC). In LF1, the alternating negative and positive inclination values denote the presence of clasts (Fig. 6B). The $\mathrm{MDF_{NRM}}$ values fluctuate between 30 and 55 mT (aside from the debris flow deposit, which shows low values with an average of approximately 45 mT (Fig. 6B)); these values indicate the presence of low coercivity minerals, such as magnetite, and a contribution from higher coercivity minerals (Tauxe & Wu 1990; Stoner *et al.* 2000).

Core 9CASQ. – Core 9CASQ is characterized by six lithofacies (Figs 6C, 7). LF2 facies forms the lower part of the core (550–362 cm) and is characterized by a succession of stratified pebbly mud with frequently deformed, diffuse to sharp, parallel laminations and some IRD (Fig. 6C). The lowermost part of LF2 reveals small peaks in mean grain size and in sorting that could be related to low turbidity current activity. Over LF2, a coarser layer of LF3 (362–340 cm) shows high density and CT number, and magnetic susceptibility values of up to ~400×10^{-5} SI (Fig. 6C). Over LF3, two distinct intervals of the LF4 facies (241–211 and 340–305 cm) consisting of a rhythmic succession of clay and silt laminae alternate with homogeneous muds without IRD (LF7; 305–275 and 125–0 cm) and layers with carbonate peaks (LF6; 211–125 cm), which can be related to BBDC.

The grain-size distribution shows relatively constant variations throughout the core, ranging from fine clay to coarse silt with an average of 4 µm, except in three distinct layers with increased average values, which correspond respectively to LF3 (362–340 cm; Figs 6C, 7, 8) and two thin layers at the base of LF2 (544–536 and 533–523 cm; Fig. 6C). These three layers are also less sorted than the rest of the core and show a normal grading typical of turbidites (Fig. 8; e.g. St-Onge *et al.* 2004; Bourget *et al.* 2011; Pouderoux *et al.* 2012). LF3 is characterized by low basal palaeomagnetic inclinations and high MAD values (Figs 6C, 8; St-Onge *et al.* 2004; Philippe 2019).

The ChRM inclination along the core generally fluctuates around the expected inclination values (I_{GAD}) and MAD values are lower than 2°, indicative of very well-defined palaeomagnetic data, except for the detrital carbonate and turbidite layers (LF6 and LF3), which have low inclination (Fig. 8) and high MAD values. Aside from LF6, the MDF_{NRM} values range between 20 and 40 mT with an average of 30 mT, which is indicative of low coercivity minerals such as magnetite (Fig. 6C). The sharp increase in MDF values in the detrital carbonate layer indicates a lower concentration of magnetite and a higher concentration of high coercivity minerals in this layer (Simon *et al.* 2012).

Magnetic properties

Day plots (Fig. 9B) indicate that most of the sediments of the three cores are composed of magnetic grains in the pseudo single domain (PSD) range with only a few samples from cores 1Comp and 9CASQ falling in the multi-domain range (MD). The samples in the MD range reflect the coarser grains observed in the rapidly deposited layers (e.g. turbidite and debrite). The magnetic k_{ARM}/k diagram (King *et al.* 1983) for the three cores indicates that the magnetic grain size is relatively fine and under 5 μm. The absolute magnetic grain-size values should be interpreted with caution because these empirical relationships were derived from synthetic magnetic grains. However, taken together with the results from the Day plot, these values suggest an optimal PSD range for palaeomagnetic reconstructions (e.g. Tauxe 1993).

The shape of the hysteresis curves of the discrete samples from the three cores is typical of low coercivity ferrimagnetic minerals such as magnetite (Fig. 9A; Tauxe *et al.* 1996; Dunlop & Özdemir 1997). In addition, the magnetic mineralogy-dependent ratio IRM/SIRM (Pseudo S-ratio) is useful for estimating changes in magnetic mineralogy, with values close to 1 indicating a low coercivity ferrimagnetic mineralogy (e.g. magnetite; St-Onge *et al.* 2003). The S-ratios in cores 77PC, 1Comp and 9CASQ, with mean values of 0.992, 0.988 and 0.987, respectively, suggest that low coercivity minerals, such as magnetite, are the dominant magnetic carriers. Moreover, the MDF_{NRM} values range from 25 to 40 mT, which also suggest the presence of magnetite and/or titanomagnetite throughout most of the three cores (Fig. 6). On the other hand, sediments of LF1 and LF6 in core 1Comp are characterized by lower MDF values that indicate the occurrence of coarser magnetic grains, as seen in the Day plot (Fig. 9B) and in the physical grain-size data (Fig. 9C). Finally, changes in the NRM, ARM, IRM and SIRM values vary by less than an order of magnitude.

Relative palaeointensity (RPI) determination and chronostratigraphy

The magnetic properties of the cores indicate that the NRM of most of the sediments, apart from RDL, is characterized by a strong, stable, single component magnetization carried by PSD magnetite grains, thus fulfilling the established criteria to derive a reliable RPI proxy (e.g. Levi & Banerjee 1976; Tauxe 1993; Stoner & St-Onge 2007; Yamazaki *et al.* 2013). Moreover, the comparison between ARM and IRM as normalizers seems to activate the same magnetic assemblages (Levi & Banerjee 1976) and the differences between the ARM and IRM as normalizers also suggest that ARM has a slightly better R^2 then IRM (Figs S4, S5). The comparison of the normalized remanence with its normalizer amongst the three cores indicates that NRM/ARM is not correlated with the ARM when rapidly deposited layers are excluded (Fig. S4). Conversely, the same comparison indicates a correlation for RDL (e.g. debrite and turbidite; LF1 and LF3) and detrital carbonates (DC) layers (LF6) with R^2 values of 0.37 and 0.40, respectively (Fig. S4). Based on these results, ARM was selected as the best normalizer. Detrital carbonate layers were then excluded from palaeomagnetic reconstructions, but RDL values, even though they do not yield appropriate results, have been retained in the figures to give the reader a glimpse of their age–depth relationship.

Discussion

RDL layers: debrite and turbidite

Glacigenic debris flow deposits are major components of TMFs (Fig. 10; Laberg & Vorren 1995; King *et al.* 1998; Vorren *et al.* 1998; Nygård *et al.* 2002). In Home Bay, LF1 is characterized by a massive, matrix-supported diamicton facies with clasts, the highest MAD values, and low values of palaeomagnetic inclinations (Fig. 6B). This combination of parameters clearly indicates that a debrite was recorded. Magnetic properties of sediments can be a source of significant information for the interpretation of sedimentary products. In fact, turbidites, debrites and detrital carbonate layers generate higher MAD values (>5°) and highly variable inclinations that move away from the expected values. If the inclination is highly variable and very low such as in LF1 or LF3 it has no geomagnetic meaning, but it indicates the presence of rapidly deposited layers (Figs 6B, C, 8).

Both the physical and magnetic profiles of core 9CASQ highlight the presence of a turbidite (LF3) in the most distal part of the Home Bay TMF (Fig. 5A). The turbidite contrasts sharply with hemipelagic muds

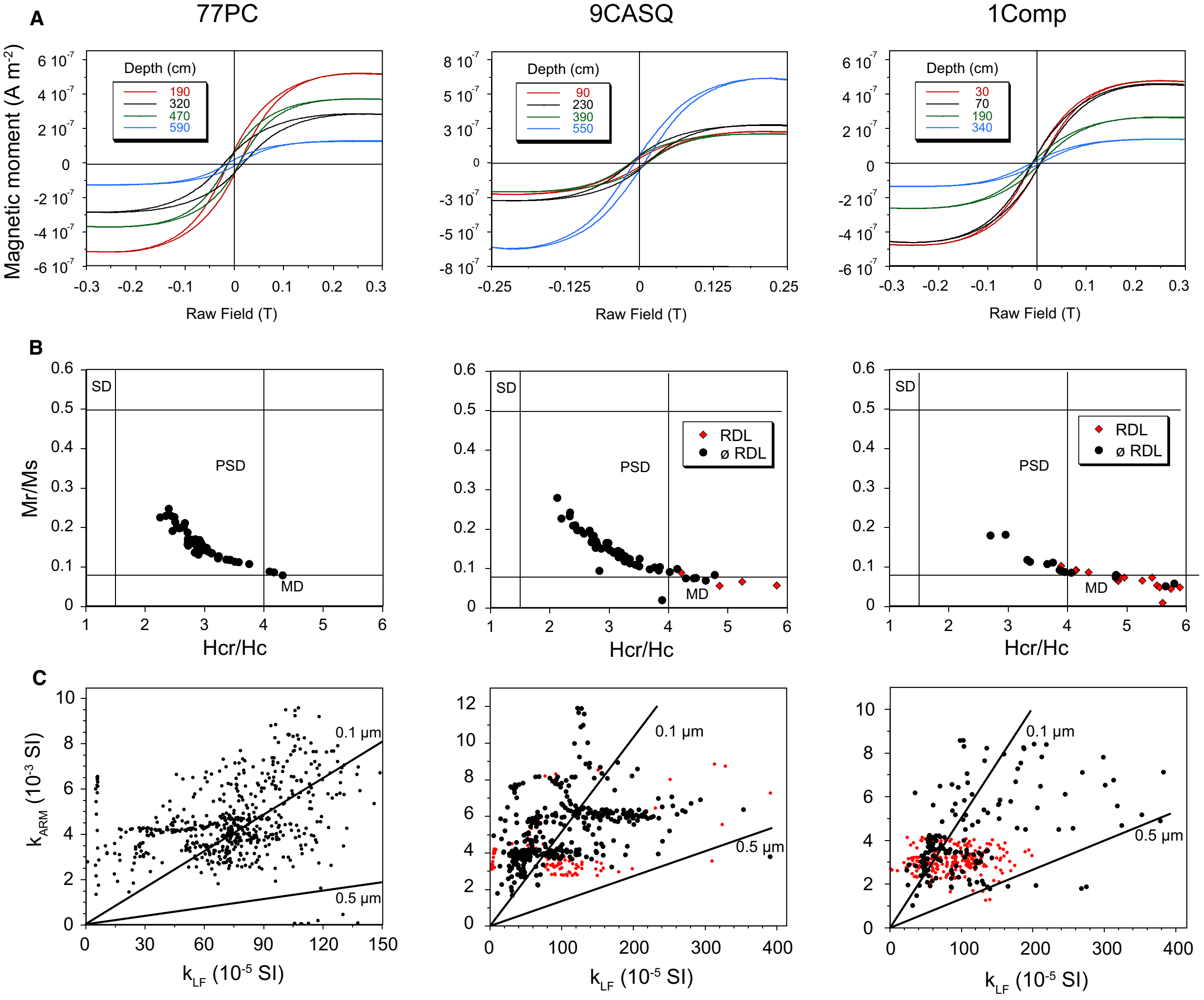

Fig. 9. A. Typical hysteresis curves and derived parameters of cores 77PC, 9CASQ and 1Comp. B. Day plot (Day *et al.* 1977). RDL = rapidly deposited layers (turbidite and debrite). C. k_{ARM} vs. k_{LF} plot representing estimated magnetic grain size for magnetite (King *et al.* 1983). Red circles represent the RDLs and black circles the remaining sediment.

and IRD layers associated with the continuous 'background' sedimentation (Figs 6B, 7). The presence of a debrite and a turbidite attests to the sensitivity of the Home Bay TMF for capturing mass wasting events on the shelf edge. The glacial debris flow reflects the presence of nearby glacial ice alike LGM sedimentary processes of other glaciated continental slopes: large debris flows were generated and accumulated down the slope on the trough-mouth fans when the local ice sheets reached the shelf break (Fig. 10; e.g. Laberg & Vorren 1995; Dowdeswell *et al.* 1996; Laberg & Vorren 1996; Vorren & Laberg 1997; King *et al.* 1998; Dowdeswell & Siegert 1999; Batchelor & Dowdeswell 2014, 2015). Subbottom profiles over the sampling location of core 1Comp (Figs 1B, 4, S6) reveal that the acoustic facies associated with the debris flow extends laterally to form a series of stacked debris flow deposits that accumulated inside this TMF (Figs 4, 10). Subglacial landforms such as MSGLs and deeply incised iceberg ploughmarks that are orientated in the trough axis also suggest that glacial ice extended near the shelf edge to later retreat while calving deep-keeled icebergs. Icebergs flowing along the BIC most likely produced iceberg ploughmark scars that are orientated N–S. However modern-day drafts of icebergs flowing through Baffin Bay rarely exceed 300 m (Praeg *et al.* 2006), indicating that they cannot account for the deep keel scours that occur below 300 m within the trough (Praeg *et al.* 2006). This suggests that the ploughmarks are not modern and that they most likely result from deep glacial ice grounding in Baffin Bay. The orientation of the ploughmarks within the trough suggests that the icebergs responsible for the deep keel erosion originated from within the trough. The ice-flow landforms (MSGLs) within the trough can be interpreted as a signature of ice-stream activity while the several channels on the TMF have probably been eroded by

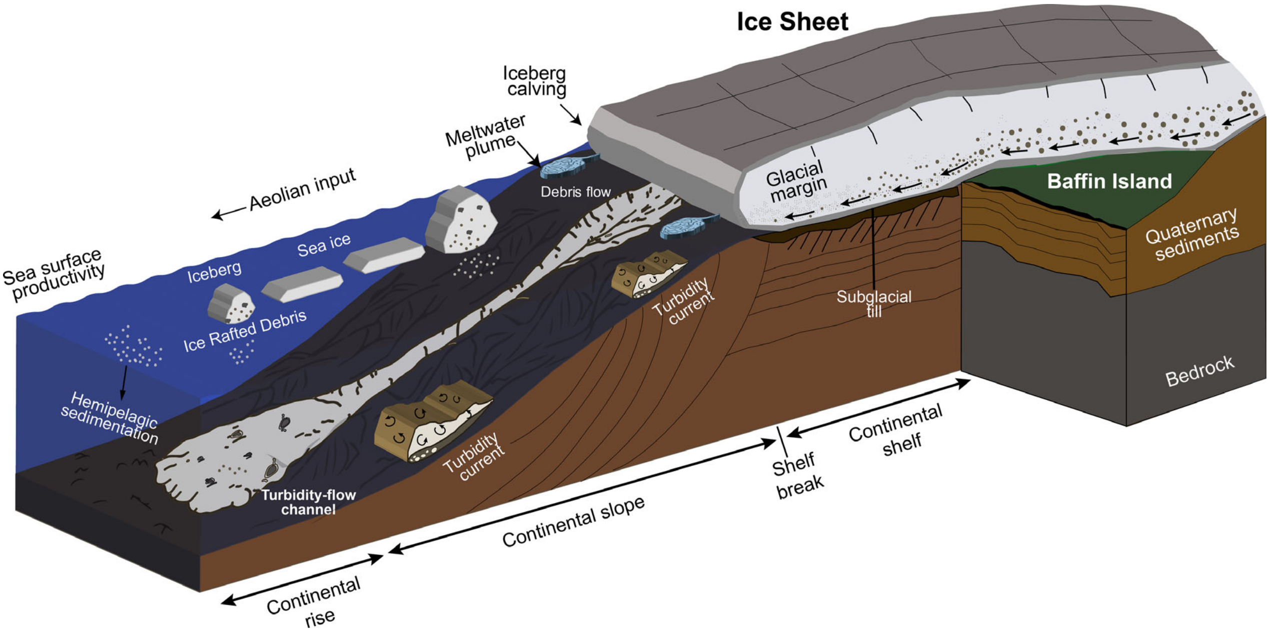

Fig. 10. Schematic model for the main glacigenic sedimentary processes inside a trough-mouth fan (TMF).

sediment-rich meltwaters from nearby glacial ice (Fig. 5B; Ottesen *et al.* 2005; Montelli *et al.* 2017). Such sediments may be transported by ice streams and be advected towards the slope where they may take the shape of debris flows (e.g. Laberg & Vorren 1995; Lasabuda *et al.* 2018) and turbidity currents. The several canyons and gullies could have formed routes for remobilizing sediments from the upper slope to their accumulation site in the basin (Figs 5A, S6; e.g. Lasabuda *et al.* 2018).

Late Quaternary Baffin Bay chronostratigraphy

While the geophysical data point towards the LIS extending near the shelf edge during the LGM, ages are needed to define whether the debrite or the turbidite is of LGM age. The three studied cores show similar RPI features that can be correlated on a regional and hemispheric scale. A combination of radiocarbon ages and palaeomagnetic tie points was used to determine the chronology of the cores. Therefore, the cores can produce a chronostratigraphical framework for the last 45 ka (Fig. 11).

A comparison between the cores and other RPI records from the Northern Hemisphere indicates that the geomagnetic origin of the signal in the 0–45 ka interval for cores 77PC, 9CASQ and 1Comp is consistent with the available radiocarbon ages (Fig. 11). Based on this comparison and the chronostratigraphy, we suggest that the debrite observed in core 1Comp was deposited before 15 cal. ka BP, while the turbidite (LF3) in 9CASQ was deposited at approximately 20 cal. ka BP. Subbottom profiles (3.5 kHz) from the coring site of core 1Comp illustrate that the core was collected on the side edge of a debris flow channel (Figs 4, 5A, S6) in a thin, side section of the channel and therefore records the full sequence since the last debris flow (i.e. since 15 ka BP). Without discarding the possibility of an earthquake in the Baffin Bay area at this time, the turbidite recorded in core 9CASQ was dated from the Last Glacial episode (~20 ka BP) and could have been triggered by the presence of the LIS margin on the continental shelf. Previous work showed that large volumes of turbidites along ice margins are related to subglacial outbursts and can be used as a proxy to determine a glaciomarine source (Dowdeswell *et al.* 1998; Hesse *et al.* 1999; Toucanne *et al.* 2012). There is still no general agreement in regards to which sedimentary structures can be used to distinguish fine-grained turbidites from contourites (Hollister 1967; Hollister & Heezen 1972; Piper 1972). Some authors contend that fine turbidite deposits such as LF3 in core 9CASQ can be differentiated from those of contourites based on certain characteristics: the absence of widespread burrowing, bioturbation, a vertical sequence of structures (Lovell & Stow 1981; Stow & Piper 1984), and traction sedimentary structures (Carter *et al.* 1996; Wynn & Stow 2002; Shanmugam 2006). These criteria are considered to be diagnostic of fine-grained turbidites rather than contourites: therefore, together with geophysical and sedimentological data, the graded sediment in LF3 is interpreted as a glacigenic turbidite.

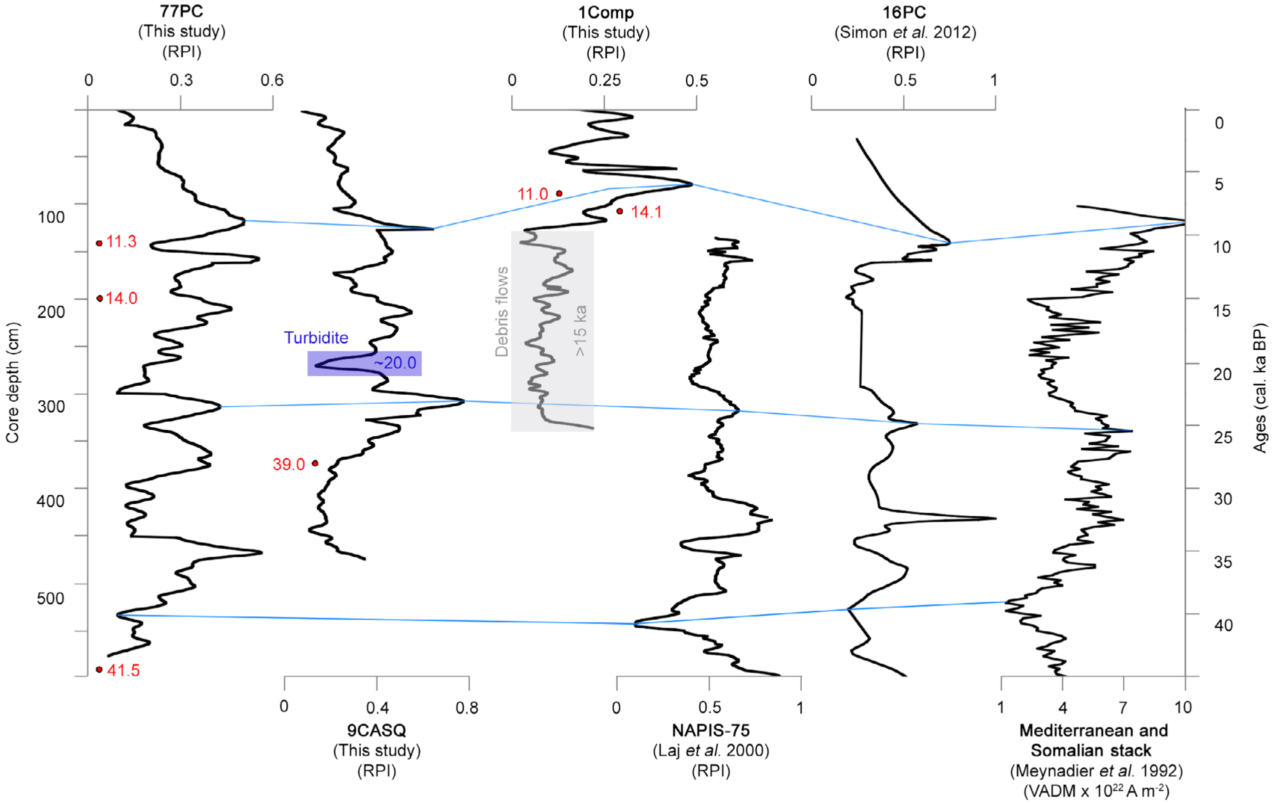

Fig. 11. Relative palaeointensity correlation. Relative palaeointensity inter-comparison for the last 45 cal. ka BP between cores 77PC (this study), 9CASQ (this study), 1Comp (this study) and RPI reference curves from the North Atlantic stack (NAPIS-75; Laj *et al.* 2000); the Baffin Bay (core 16PC; Simon *et al.* 2012) and the Mediterranean and Somalian Stack (Meynadier *et al.* 1992). The correlative palaeointensity features are indicated with the blue lines. RDLs (e.g. debrite and turbidite) are delimited by the grey and purple rectangles. In red, calibrated radiocarbon ages (cal. ka BP). Radiocarbon ages from core HU2013-029-0077 are from Jenner *et al.* (2018). Here, various scales are used to highlight the trends.

The occurrence of >15 000-year-old GDFs and turbidity current deposits on the Home Bay TMF together with glacial lineations clearly indicate that the LIS advanced near the shelf edge during the Last Glacial episode. According to several authors, the maximum extension of the LIS in the Home Bay area probably lasted up to ~14–12 cal. ka BP (Dyke *et al.* 2002; Margold *et al.* 2015). The chronostratigraphy obtained by a combination of palaeomagnetism and radiocarbon ages shows that debrites were being deposited in the Home Bay TMF until around 15 cal. ka BP, which approximately marks the beginning of the Bølling warm period (Deschamps *et al.* 2012). Hence, perennial temperatures and precipitation during the post-LGM and pre-Bølling periods were cold and/or precipitation high enough to keep the ice margin near the shelf edge. This late retreat of the LIS margin offshore Home Bay is somewhat similar to persistent glacial ice in southern regions (e.g. Des Moines lobe, James Bay lobe, and Great Lakes lobes; Dyke 2004), which only shows significant retreat after 15 cal. ka BP. This pattern may point to a similar response of the LIS to the Bølling warming over all its extent.

Conclusions

New geomorphological, stratigraphical and sediment core data coupled with the dating of glacigenic debrite and turbidite allowed us to reconstruct the activity of the LIS margin in the Home Bay trough and trough-mouth fan during the Last Glacial episode. The following results suggest that an ice margin extended near the shelf edge of Home Bay during the Last Glacial episode:

- Seven lithofacies within the cores depict a full glacial-deglacial-postglacial sedimentary sequence: (i) rapidly deposited layers such as a debrite and a turbidite generated in a glacial environment; (ii) sediments from meltwater plumes, turbidity currents and possibly bottom currents generated in an ice-proximal environment; (iii) ice-rafted debris deposited since the last deglaciation; and (iv) postglacial hemipelagic sediments.
- The chronostratigraphy from the core 9CASQ indicates that the turbidite observed was probably transported along the slope of the Home Bay TMF during the LGM.

- High-resolution swath bathymetry data allowed the identification of subglacial landforms related to ice-stream activity near the shelf edge. The subglacial landforms, such as MSGLs, together with the age of the debrite and the turbidite, indicate that glacial processes have eroded and moulded the shelf during and since the LGM.

Finally, this paper outlines the usefulness of combining palaeomagnetic measurements with radiocarbon dating for establishing a reliable chronostratigraphy in an environment where calcium carbonate dissolution challenges the use of foraminifera for dating.

Index of abbreviations

TMF = trough-mouth fan; GDF = glacigenic debris flows; LIS = Laurentide Ice Sheet; IIS = Innuitian Ice Sheet; GIS = Greenland Ice Sheet; LGM = Last Glacial Maximum; BIC = Baffin Island Current; 9CASQ = AMD16-LGM-09; 1Comp = AMD0217-01PC and AMD0217-01TWC; 77PC = HU2013-029-0077; LF1 to LF7 = Lithofacies 1 to 7; RDL = rapidly deposited layer; BBDC = Baffin Bay detrital carbonates; GZW = grounding-zone wedge; MSGL = mega-scale glacial lineation; MSCL = Multi Sensor Core Logger; XRF = X-ray fluorescence. Palaeomagnetic parameters: k_{LF} = magnetic susceptibility; NRM = natural remanent magnetization; ARM = anhysteretic remanent magnetization; IRM = isothermal remanent magnetization; SIRM = saturation isothermal magnetization; ChRM = characteristic remanent magnetization; MAD = maximum angular deviation; MDF = median destructive field; I_{GAD} = axial dipole model; PSD = pseudo single domain; SD = single domain; PSV = palaeomagnetic secular variation; RPI = relative palaeointensity; Ms = saturation magnetization; Hc = coercive force; Mrs = saturation remanence; Hcr = coercivity of remanence; AMS = accelerator mass spectrometry; AGM = alternating gradient force magnetometer; AF = alternating field; DC = direct current.

Acknowledgements. – We thank Calvin Campbell from the Geological Survey of Canada for access to core 77PC and its radiocarbon ages. We also sincerely thank the captains, officers, crew and scientists on board of CCGS 'Amundsen' for the recovery of the cores used in this study. We also thank Quentin Beauvais (ISMER) and Marie-Pier St-Onge (ISMER) for their technical support and advice in the laboratory as well as Jean-Carlos Montero-Serrano (ISMER) for his help collecting several of the cores studied. This research was funded by the ArcticNet Network of Centres of Excellence of Canada and by the Natural Sciences and Engineering Research Council of Canada (NSERC) through Discovery grants to G. St-Onge and P. Lajeunesse. Finally, we are thankful to the editor Jan A. Piotrowski, Calvin Campbell, Kimberley Jenner and Amando Lasabuda for providing constructive comments that helped to improve the manuscript.

Author contributions. – YL performed the laboratory measurements, processed and analysed the data, wrote the various versions of the manuscript and made the figures; GS designed and supervised all the measurements and writing; PL was responsible for the 2016 and 2017 CCGS 'Amundsen' expeditions and supervised the geophysical aspects of the manuscript and writing. PAD contributed to the geophysical data processing and analyses as well as preparation of related figures. EB contributed to the interpretation of the geomorphological data and glacial dynamics in Baffin Bay and to the final version of the manuscript. The other authors contributed to all the various versions of the manuscript.

References

Aksu, A. E. & Piper, D. J. W. 1987: Late Quaternary sedimentation in Baffin Bay. *Canadian Journal of Earth Sciences 24*, 1833–1846.

Andrews, J. T. 1985: *Quaternary Environments: Eastern Canadian Arctic, Baffin Bay and Western Greenland*. 774 pp. Allen & Unwin, Boston.

Andrews, J. T. & Jennings, A. E. 1990: Geomagnetic secular variations (inclination) of high-latitude fjord cores—Eastern Canadian Arctic. *Polar Research 8*, 245–259.

Andrews, J. T., Jennings, A. E., MacLean, B., Mudie, P. J., Praeg, D. & Vilks, G. 1991: The surficial geology of the Canadian eastern Arctic and Polar continental shelves. *Continental Shelf Research 11*, 791–819.

Andrews, J. T., Kirby, M., Jennings, A. & Barber, D. 1998: Late Quaternary stratigraphy, chronology, and depositional processes on the slope of SE Baffin Island, detrital carbonate and Heinrich events: implications for onshore glacial history. *Géographie physique et Quaternaire 52*, 91–105.

Andrews, J. T., Kirby, M., Jennings, A. E. & Barber, D. C. 2009: Late Quaternary stratigraphy, chronology, and depositional processes on the slope of S. E. Baffin Island, detrital carbonate and Heinrich events: implications for onshore glacial history. *Géographie physique et Quaternaire 52*, 91–105.

Balsam, W. L., Deaton, B. C. & Damuth, J. E. 1999: Evaluating optical lightness as a proxy for carbonate content in marine sediment cores. *Marine Geology 161*, 141–153.

Barletta, F., St-Onge, G., Channell, J. E. T. & Rochon, A. 2010: Dating of Holocene western Canadian Arctic sediments by matching palaeomagnetic secular variation to a geomagnetic field model. *Quaternary Science Reviews 29*, 2315–2324.

Barletta, F., St-Onge, G., Channell, J. E. T., Rochon, A., Polyak, L. & Darby, D. 2008: High-resolution palaeomagnetic secular variation and relative palaeointensity records from the western Canadian Arctic: implication for Holocene stratigraphy and geomagnetic field behaviour. *Canadian Journal of Earth Sciences 45*, 1265–1281.

Batchelor, C. L. & Dowdeswell, J. A. 2014: The physiography of High Arctic cross-shelf troughs. *Quaternary Science Reviews 92*, 68–96.

Batchelor, C. L. & Dowdeswell, J. A. 2015: Ice-sheet grounding-zone wedges (GZWs) on high-latitude continental margins. *Marine Geology 363*, 65–92.

Bourget, J., Zaragosi, S., Ellouz-Zimmermann, N., Mouchot, N., Garlan, T., Schneider, J.-L., Valentine, L. & Lallemant, S. 2011: Turbidite system architecture and sedimentary processes along topographically complex slopes: the Makran convergent margin. *Sedimentology 58*, 376–406.

Briner, J. P., Michelutti, N., Francis, D. R., Miller, G. H., Axford, Y., Wooller, M. J. & Wolfe, A. P. 2006a: A multi-proxy lacustrine record of Holocene climate change on northeastern Baffin Island, Arctic Canada. *Quaternary Research 65*, 431–442.

Briner, J. P., Miller, G. H., Davis, P. T. & Finkel, R. C. 2005: Cosmogenic exposure dating in arctic glacial landscapes: implications for the glacial history of northeastern Baffin Island, Arctic Canada. *Canadian Journal of Earth Sciences 42*, 67–84.

Briner, J. P., Miller, G. H., Davis, P. T. & Finkel, R. C. 2006b: Cosmogenic radionuclides from fiord landscapes support differential erosion by overriding ice sheets. *Geological Society of America Bulletin 118*, 406–420.

Brouard, E. & Lajeunesse, P. 2017: Maximum extent and decay of the Laurentide Ice Sheet in Western Baffin Bay during the last glacial episode. *Scientific Reports 7*, 10711, https://doi.org/10.1038/s41598-017-11010-9.

Brouard, E. & Lajeunesse, P. 2019a: Glacial to postglacial submarine landform assemblages in fiords of northeastern Baffin Island. *Geomorphology 330*, 40–56.

Brouard, E. & Lajeunesse, P. 2019b: Submarine geomorphology of the northeastern Baffin Island fiords and cross-shelf troughs. *Journal of Maps 15*, 662–676.

Campbell, D. C. 2014: CCGS Hudson Expedition 2013-029. Geological hazard assessment of Baffin Bay and biodiversity assessment of Hatton Basin. *Geological Survey of Canada, Open file 7594*, 124 pp.

Campbell, D. C. & Bennett, J. R. 2014: Preliminary results from recent investigations of marine geological hazards in Baffin Bay, Nunavut and Greenland. *Canada-Nunavut Geoscience Office, Summary of Activities 2013*, 121–128.

Carter, R. M., Carter, L. & McCave, I. N. 1996: Current controlled sediment deposition from the shelf to the deep ocean: the Cenozoic evolution of circulation through the SW Pacific gateway. *Geologische Rundschau 85*, 438–451.

Channell, J. E. T., Hodell, D. A., Romero, O., Hillaire-Marcel, C., de Vernal, A., Stoner, J. S., Mazaud, A. & Röhl, U. 2012: A 750-kyr detrital-layer stratigraphy for the North Atlantic (IODP Sites U1302—U1303, Orphan Knoll, Labrador Sea). *Earth and Planetary Science Letters 317*, 218–230.

Clark, C. D. 1993: Mega-scale glacial lineations and cross-cutting ice-flow landforms. *Earth Surface Processes and Landforms 18*, 1–29.

Coulthard, R. D., Furze, M. F. A., Pieńkowski, A. J., Nixon, F. C. & England, J. H. 2010: New marine ΔR values for Arctic Canada. *Quaternary Geochronology 5*, 419–434.

Cowan, E. A. & Powell, R. D. 1990: Suspended sediment transport and deposition of cyclically interlaminated sediment in a temperate glacial fjord, Alaska, USA. *Geological Society, London, Special Publications 53*, 75–89.

Cowan, E. A., Cai, J., Powell, R. D., Clark, J. D. & Pitcher, J. N. 1997: Temperate glacimarine varves: an example from Disenchantment Bay, southern Alaska. *Journal of Sedimentary Research 67*, 536–549.

Day, R., Fuller, M. & Schmidt, V. A. 1977: Hysteresis properties of titanomagnetites: grain-size and compositional dependence. *Physics of the Earth and Planetary Interiors 13*, 260–267.

De Blasio, F. V., Elverhøi, A., Issler, D., Harbitz, C. B., Bryn, P. & Lien, R. 2004: Flow models of natural debris flows originating from overconsolidated clay materials. *Marine Geology 213*, 439–455.

Deschamps, P., Durand, N., Bard, E., Hamelin, B., Camoin, G., Thomas, A. L. & Yokoyama, Y. 2012: Ice-sheet collapse and sea-level rise at the Bølling warming 14,600 years ago. *Nature 483*, 559–564.

Domack, E. W. 1990: Laminated terrigenous sediments from the Antarctic Peninsula: the role of subglacial and marine processes. *Geological Society, London, Special Publications 53*, 91–103.

Dowdeswell, J. A. & Cromack, M. 1991: Behavior of a glacier-derived suspended sediment plume in a small Arctic inlet. *The Journal of Geology 99*, 111–123.

Dowdeswell, J. A. & Siegert, M. J. 1999: Ice-sheet numerical modeling and marine geophysical measurements of glacier-derived sedimentation on the Eurasian Arctic continental margins. *Geological Society of America Bulletin 111*, 1080–1097.

Dowdeswell, J. A. & Vásquez, M. 2013: Submarine landforms in the fjords of southern Chile: implications for glacimarine processes and sedimentation in a mild glacier-influenced environment. *Quaternary Science Reviews 64*, 1–19.

Dowdeswell, J. A., Elverhøi, A. & Spielhagen, R. 1998: Glacimarine sedimentary processes and facies on the polar North Atlantic margins. *Quaternary Science Reviews 17*, 243–272.

Dowdeswell, J. A., Kenyon, N. H., Elverhøi, A., Laberg, J. S., Hollender, F., Mienert, J. & Siegert, M. J. 1996: Large-scale sedimentation on the glacier-influenced polar North Atlantic Margins: long-range side-scan sonar evidence. *Geophysical Research Letters 23*, 3535–3538.

Dowdeswell, J. A., Ó Cofaigh, C., Noormets, R., Larter, R. D., Hillenbrand, C.-D., Benetti, S., Evans, J. & Pudsey, C. J. 2008: A major trough-mouth fan on the continental margin of the Bellingshausen Sea, West Antarctica: the Belgica Fan. *Marine Geology 252*, 129–140.

Dowdeswell, J. A., Whittington, R. J., Jennings, A. E., Andrews, J. T., Mackensen, A. & Marienfeld, P. 2000: An origin for laminated glacimarine sediments through sea-ice build-up and suppressed iceberg rafting. *Sedimentology 47*, 557–576.

Dunlap, E. & Tang, C. C. L. 2006: Modelling the mean circulation of Baffin Bay. *Atmosphere-Ocean 44*, 99–109.

Dunlop, D. J. & Özdemir, Ö. 1997: *Rock Magnetism. Fundamental and Frontiers.* 573 pp. Cambridge University Press, Cambridge.

Dyke, A. 2004: An outline of the deglaciation of North America with emphasis on central and northern Canada. *Developments in Quaternary Sciences 2*, 373–424.

Dyke, A. & Prest, V. 1987: Late Wisconsinan and Holocene history of the Laurentide ice sheet. *Géographie physique et Quaternaire 41*, 237–263.

Dyke, A. S., Andrews, J. T., Clark, P. U., England, J. H., Miller, G. H., Shaw, J. & Veillette, J. J. 2002: The Laurentide and Innuitian ice sheets during the last glacial maximum. *Quaternary Science Reviews 21*, 9–31.

Funder, S., Kjeldsen, K. K., Kjær, K. H. & Ó Cofaigh, C. 2011: The Greenland Ice Sheet during the past 300,000 years: a review. *Developments in Quaternary Sciences 15*, 699–713.

Hesse, R., Khodabakhsh, S., Klaucke, I. & Ryan, W. B. F. 1997: Asymmetrical turbid surface-plume deposition near ice-outlets of the Pleistocene Laurentide ice sheet in the Labrador Sea. *Geo-Marine Letters 17*, 179–187.

Hesse, R., Klauck, I., Khodabakhsh, S. & Piper, D. 1999: Continental slope sedimentation adjacent to an ice margin. III. The upper Labrador Slope. *Marine Geology 155*, 249–276.

Hiscott, R. N. & Aksu, A. E. 1994: Submarine debris flows and continental slope evolution in front of Quaternary ice sheets, Baffin Bay, Canadian Arctic. *AAPG Bulletin 78*, 445–460.

Hiscott, R. N., Aksu, A. E. & Nielsen, O. B. 1989: Provenance and dispersal patterns, Pliocene-Pleistocene section at site 645, Baffin Bay. *Proceedings of the Ocean Drilling Program, Scientific Results 105*, 31–52.

Hodell, D. A., Channell, J. E. T., Curtis, J. H., Romero, O. E. & Röhl, U. 2008: Onset of "Hudson Strait" Heinrich events in the eastern North Atlantic at the end of the middle Pleistocene transition (~ 640 ka)? *Palaeoceanography 23*, PA4218, https://doi.org/10.1029/2008pa001591.

Hollister, C. D. 1967: *Sediment distribution and deep circulation in the western North Atlantic.* Ph.D. thesis, Columbia University.

Hollister, C. D. & Heezen, B. C. 1972: Geologic effects of ocean bottom currents. *In* Gordon, A. L. (ed.): *Studies in Physical Oceanography: A Tribute to George Wust on his 80th Birthday*, 37–66. Gordon & Breach, New York.

Jackson, R., Carlson, A. E., Hillaire-Marcel, C., Wacker, L., Vogt, C. & Kucera, M. 2017: Asynchronous instability of the North American-Arctic and Greenland ice sheets during the last deglaciation. *Quaternary Science Reviews 164*, 140–153.

Jakobsson, M., Mayer, L., Coakley, B., Dowdeswell, J. A., Forbes, S., Fridman, B., Hodnesdal, H., Noormets, R., Pedersen, R., Rebesco, M., Werner, H. S., Zarayskaya, Y., Accettella, D., Armstrong, A, Anderson, R. M., Bienhoff, P., Camerlenghi, A., Church, I., Edwards, M., MGardner, J. V., Hall, J. K., Hell, B., Hestvik, O., Kristoffersen, Y., Marcussen, C., Mohammad, R., Mosher, D., Nghiem, S. V., Pedrosa, M. T., Travaglini, P. G., Weatherall, P. 2012: The international bathymetric chart of the Arctic Ocean (IBCAO) version 3.0. *Geophysical Research Letters 39*, L12609.

Jenner, K. A., Campbell, D. C. & Piper, D. J. W. 2018: Along-slope variations in sediment lithofacies and depositional processes since the Last Glacial Maximum on the northeast Baffin margin, Canada. *Marine Geology 405*, 92–107.

Jennings, A. 1993: The Quaternary history of Cumberland Sound, southeastern Baffin Island: the marine evidence. *Géographie physique et Quaternaire 47*, 21–42.

King, J. W., Banerjee, S. K. & Marvin, J. 1983: A new rock-magnetic approach to selecting sediments for geomagnetic palaeointensity studies: application to palaeointensity for the last 4000 years. *Journal of Geophysical Research: Solid Earth 88*, 5911–5921.

King, E. L., Haflidason, H. & Sejrup, H. P. 1998: Glacigenic debris flows on the North Sea Trough Mouth Fan during ice stream maxima. *Marine Geology 152*, 217–246.

Laberg, J. S. & Vorren, T. O. 1995: Late Weichselian submarine debris flow deposits on the Bear Island Trough Mouth Fan. *Marine Geology 127*, 45–72.

Laberg, J. S. & Vorren, T. O. 1996: The middle and late Pleistocene evolution and the Bear Island trough mouth fan. *Global and Planetary Change 12*, 309–330.

Laj, C., Kissel, C., Mazaud, A., Channell, J. E. T. & Beer, J. 2000: North Atlantic palaeointensity stack since 75ka (NAPIS—75) and the duration of the Laschamp event. *Philosophical Transactions of the Royal Society of London A: Mathematical, Physical and Engineering Sciences 358*, 1009–1025.

Lasabuda, A., Geissler, W. H., Laberg, J. S., Knutsen, S., Rydningen, T. A. & Berglar, K. 2018: Late Cenozoic erosion estimates for the northern Barents Sea: quantifying glacial sediment input to the Arctic Ocean. *Geochemistry, Geophysics, Geosystems 19*, 4876–4903.

Ledu, D., Rochon, A., de Vernal, A. & St-Onge, G. 2008: Palynological evidence of Holocene climate change in the eastern Arctic: a possible shift in the Arctic oscillation at the millennial time scale. *Canadian Journal of Earth Sciences 45*, 1363–1375.

Levi, S. & Banerjee, S. K. 1976: On the possibility of obtaining relative palaeointensities from lake sediments. *Earth and Planetary Science Letters 29*, 219–226.

Li, G., Piper, D. J. W. & Calvin Campbell, D. 2011: The Quaternary Lancaster Sound trough-mouth fan, NW Baffin Bay. *Journal of Quaternary Science 26*, 511–522.

Li, G., Piper, D. J. W., Campbell, D. C. & Mosher, D. 2012: Turbidite deposition and the development of canyons through time on an intermittently glaciated continental margin: the Bonanza Canyon system, offshore eastern Canada. *Marine and Petroleum Geology 29*, 90–103.

Lovell, J. P. B. & Stow, D. A. V. 1981: Identification of ancient sandy contourites. *Geology 9*, 347–349.

Lucchi, R. G., Camerlenghi, A., Rebesco, M., Colmenero-Hidalgo, E., Sierro, F. J., Sagnotti, L., Urgeles, R., Melis, R., Morigi, C., Bárcena, M.-A., Giorgetti, G., Villa, G., Persico, D., Flores, J.-A., Rigual-Hernández, A. S., Pedrosa, M. T., Macri, P. & Caburlotto, A. 2013: Postglacial sedimentary processes on the Storfjorden and Kveithola trough mouth fans: significance of extreme glacimarine sedimentation. *Global and Planetary Change 111*, 309–326.

Margold, M., Stokes, C. R. & Clark, C. D. 2015: Ice streams in the Laurentide Ice Sheet: identification, characteristics and comparison to modern ice sheets. *Earth-Science Review 143*, 117–146.

Mazaud, A. 2005: User-friendly software for vector analysis of the magnetization of long sediment cores. *Geochemistry, Geophysics, Geosystems 6*, 3113–3115.

McKay, J. L., de Vernal, A., Hillaire-Marcel, C., Not, C., Polyak, L. & Darby, D. 2008: Holocene fluctuations in Arctic sea-ice cover: dinocyst-based reconstructions for the eastern Chukchi Sea. *Canadian Journal of Earth Sciences 45*, 1377–1397.

Meynadier, L., Valet, J.-P., Weeks, R., Shackleton, N. J. & Hagee, V. L. 1992: Relative geomagnetic intensity of the field during the last 140 ka. *Earth and Planetary Science Letters 114*, 39–57.

Montelli, A., Dowdeswell, J. A., Ottesen, D. & Johansen, S. E. 2017: Ice-sheet dynamics through the Quaternary on the mid-Norwegian continental margin inferred from 3D seismic data. *Marine and Petroleum Geology 80*, 228–242.

Nygård, A., Sejrup, H. P., Haflidason, H. & King, E. L. 2002: Geometry and genesis of glacigenic debris flows on the North Sea Fan: TOBI imagery and deep-tow boomer evidence. *Marine Geology 188*, 15–33.

Ó Cofaigh, C., Andrews, J. T., Jennings, A. E., Dowdeswell, J. A., Hogan, K. A., Kilfeather, A. A. & Sheldon, C. 2013: Glacimarine lithofacies, provenance and depositional processes on a West Greenland trough-mouth fan. *Journal of Quaternary Science 28*, 13–26.

Ó Cofaigh, C., Taylor, J., Dowdeswell, J. A. & Pudsey, C. J. 2003: Palaeo-ice streams, trough mouth fans and high-latitude continental slope sedimentation. *Boreas 32*, 37–55.

Ottesen, D., Dowdeswell, J. A. & Rise, L. 2005: Submarine landforms and the reconstruction of fast-flowing ice streams within a large Quaternary ice sheet: the 2500-km-long Norwegian-Svalbard margin (57–80 N). *Geological Society of America Bulletin 117*, 1033–1050.

Philippe, É. G. H. 2019: *Acquisition de l'aimantation remanente dans les sediments.* Ph.D. thesis, Université du Québec à Rimouski.

Philippe, É. G. H., Valet, J., St-Onge, G. & Thevarasan, A. 2018: Are palaeomagnetic records from U-channels appropriate for studies of reversals and excursions? *Geochemistry, Geophysics, Geosystems 19*, 4130–4142.

Piper, D. J. W. 1972: Sediments of the Middle Cambrian Burgess Shale, Canada. *Lethaia 5*, 169–175.

Pouderoux, H., Proust, J.-N., Lamarche, G., Orpin, A. & Neil, H. 2012: Postglacial (after 18 ka) deep-sea sedimentation along the Hikurangi subduction margin (New Zealand): characterisation, timing and origin of turbidites. *Marine Geology 295*, 51–76.

Praeg, D. B., MacLean, B. & Sonnichsen, G. V. 2006: Quaternary geology of the northeast Baffin Island continental shelf, Cape Aston to Buchan Gulf (70° to 72° N). *Geological Survey of Canada, Open File 5409*, 98 pp.

Reimer, P. J., Bard, E., Bayliss, A., Beck, J. W., Blackwell, P. G., Bronk Ramsey, C., Buck, C. E., Edwards, R. L., Friedrich, M., Grootes, P. M., Guilderson, T. P., Haflidason, H., Hajdas, I., Hatté, C., Heaton, T. J., Hogg, A. G., Hughen, K. A., Kaiser, K. F., Kromer, B., Manning, S. W., Reimer, R. W., Richards, D. A., Scott, E. M., Southon, J. R., Turney, C. S. M. & Plicht, J. 2013: IntCal13 and MARINE13 radiocarbon age calibration curves 0-50,000 years cal BP. *Radiocarbon 55*, 1869–1887.

Roger, J., Saint-Ange, F., Lajeunesse, P., Duchesne, M. J. & St-Onge, G. 2013: Late Quaternary glacial history and meltwater discharges along the Northeastern Newfoundland Shelf. *Canadian Journal of Earth Sciences 50*, 1178–1194.

Shanmugam, G. 2006: *Deep-water Processes and Facies Models: Implications for Sandstone Petroleum Reservoirs.* 496 pp. Elsevier, Amsterdam.

Simon, Q., Hillaire-Marcel, C., St-Onge, G. & Andrews, J. T. 2014: North-eastern Laurentide, western Greenland and southern Innuitian ice stream dynamics during the last glacial cycle. *Journal of Quaternary Science 29*, 14–26.

Simon, Q., St-Onge, G. & Hillaire-Marcel, C. 2012: Late Quaternary chronostratigraphic framework of deep Baffin Bay glaciomarine sediments from high-resolution paleomagnetic data. *Geochemistry, Geophysics, Geosystems 13*, Q0AO03, https://doi.org/10.1029/2012gc004272.

Simon, Q., Thouveny, N., Bourles, D. L., Nuttin, L., Hillaire-Marcel, C. & St-Onge, G. 2016: Authigenic 10Be/9Be ratios and 10Be-fluxes (230Thxs-normalized) in central Baffin Bay sediments during the last glacial cycle: Paleoenvironmental implications. *Quaternary Science Reviews 140*, 142–162.

Snowball, I. & Muscheler, R. 2007: Palaeomagnetic intensity data: an Achilles heel of solar activity reconstructions. *The Holocene 17*, 851–859.

Snowball, I. & Sandgren, P. 2002: Geomagnetic field variations in northern Sweden during the Holocene quantified from varved lake sediments and their implications for cosmogenic nuclide production rates. *The Holocene 12*, 517–530.

Stanley, S. & Luczaj, J. A. 2015: *Earth System History.* 624 pp. Macmillan, New York.

Stokes, C. R. 2017: Deglaciation of the Laurentide Ice Sheet from the Last Glacial Maximum. *Cuadernos de Investigación Geográfica 43*, 377–428.

Stokes, C. R. & Clark, C. D. 2002: Are long subglacial bedforms indicative of fast ice flow? *Boreas 31*, 239–249.

Stoner, J. S. & St-Onge, G. 2007: Magnetic stratigraphy in palaeoceanography: reversals, excursions, palaeointensity, and secular variation. *Developments in Marine Geology 1*, 99–138.

Stoner, J. S., Channell, J. E. T., Hillaire-Marcel, C. & Kissel, C. 2000: Geomagnetic palaeointensity and environmental record from Labrador Sea core MD95–2024: global marine sediment and ice core chronostratigraphy for the last 110 kyr. *Earth and Planetary Science Letters 183*, 161–177.

St-Onge, G. & Stoner, J. S. 2011: Palaeomagnetism near the north magnetic pole. *Oceanography 24*, 162–173.

St-Onge, G., Mulder, T., Francus, P. & Long, B. 2007: Continuous physical properties of cored marine sediments. *Developments in Marine Geology 1*, 63–98.

St-Onge, G., Mulder, T., Piper, D. J. W., Hillaire-Marcel, C. & Stoner, J. S. 2004: Earthquake and flood-induced turbidites in the Saguenay Fjord (Québec): a Holocene palaeoseismicity record. *Quaternary Science Reviews 23*, 283–294.

St-Onge, G., Stoner, J. S. & Hillaire-Marcel, C. 2003: Holocene palaeomagnetic records from the St. Lawrence Estuary, eastern Canada: centennial- to millennial-scale geomagnetic modulation of cosmogenic isotopes. *Earth and Planetary Science Letters 209*, 113–130.

Stow, D. A. V. & Piper, D. J. W. 1984: Deep-water fine-grained sediments: facies models. *Geological Society, London, Special Publications 15*, 611–646.

Stuiver, M., Reimer, P. J. & Reimer, R. W. 2017: *CALIB 7.1*. Available at: http://calib.org.

Syvitski, J. P. M. 1989: On the deposition of sediment within glacier-influenced fjords: oceanographic controls. *Marine Geology 85*, 301–329.

Syvitski, J. P. & Shaw, J. 1995: Sedimentology and geomorphology of fjords. *Developments in Sedimentology 53*, 113–178.

Syvitski, J. P., Burrell, D. C. & Skei, J. M. 2012: *Fjords: Processes and Products.* 379 pp. Springer Science & Business Media, New York.

Tang, C. C. L., Ross, C. K., Yao, T., Petrie, B., DeTracey, B. M. & Dunlap, E. 2004: The circulation, water masses and sea-ice of Baffin Bay. *Progress in Oceanography 63*, 183–228.

Tanty, C., Valet, J., Carlut, J., Bassinot, F. & Zaragosi, S. 2016: Acquisition of detrital magnetization in four turbidites. *Geochemistry, Geophysics, Geosystems 17*, 3207–3223.

Tauxe, L. 1993: Sedimentary records of relative palaeointensity of the geomagnetic field: theory and practice. *Reviews of Geophysics 31*, 319–354.

Tauxe, L. 2010: *Essentials of Palaeomagnetism*. 489 pp. University of California Press, Berkeley.

Tauxe, L. & Wu, G. 1990: Normalized remanence in sediments of the western equatorial Pacific: relative palaeointensity of the geomagnetic field? *Journal of Geophysical Research: Solid Earth 95*, 12337–12350.

Tauxe, L., Mullender, T. A. T. & Pick, T. 1996: Potbellies, wasp-waists, and superparamagnetism in magnetic hysteresis. *Journal of Geophysical Research: Solid Earth 101*, 571–583.

Toucanne, S., Zaragosi, S., Bourillet, J. F., Dennielou, B., Jorry, S. J., Jouet, G. & Cremer, M. 2012: External controls on turbidite sedimentation on the glacially-influenced Armorican margin (Bay of Biscay, western European margin). *Marine Geology 303–306*, 137–153.

Tripsanas, E. K. & Piper, D. J. W. 2008: Late Quaternary stratigraphy and sedimentology of Orphan Basin: implications for meltwater dispersal in the southern Labrador Sea. *Palaeogeography, Palaeoclimatology, Palaeoecology 260*, 521–539.

de Vernal, A., Bilodeau, G., Hillaire-Marcel, C. & Kassou, N. 1992: Quantitative assessment of carbonate dissolution in marine sediments from foraminifer linings vs. shell ratios: Davis Strait, northwest North Atlantic. *Geology 20*, 527–530.

de Vernal, A., Hillaire-Marcel, C., Aksu, A. E. & Mudie, P. J. 1987: Palynostratigraphy and chronostratigraphy of Baffin Bay deep sea cores: climatostratigraphic implications. *Palaeogeography, Palaeoclimatology, Palaeoecology 61*, 97–105.

Vorren, T. O. & Laberg, J. S. 1997: Trough mouth fans—Palaeoclimate and ice-sheet monitors. *Quaternary Science Reviews 16*, 865–881.

Vorren, T. O., Laberg, J. S., Blaume, F., Dowdeswell, J. A., Kenyon, N. H., Mienert, J., Rumohr, J. & Werner, F. 1998: The Norwegian—Greenland Sea continental margins: morphology and late Quaternary sedimentary processes and environment. *Quaternary Science Reviews 17*, 273–302.

Winsor, K., Carlson, A. E., Klinkhammer, G. P., Stoner, J. S. & Hatfield, R. G. 2012: Evolution of the northeast Labrador Sea during the last interglaciation. *Geochemistry, Geophysics, Geosystems 13*, Q11006, https://doi.org/10.1029/2012gc004263.

Wynn, R. B. & Stow, D. A. V. 2002: Classification and characterisation of deep-water sediment waves. *Marine Geology 192*, 7–22.

Yamazaki, T., Yamamoto, Y., Acton, G., Guidry, E. P. & Richter, C. 2013: Rock-magnetic artifacts on long-term relative paleointensity variations in sediments. *Geochemistry, Geophysics, Geosystems 14*, 29–43.

Supporting Information

Additional Supporting Information may be found in the online version of this article at http://www.boreas.dk.

Fig. S1. Line 76029_AG_280_1730 (airgun profile) collected in 1976 on board the CCGS 'Hudson' by the Geological Survey of Canada.

Fig. S2. Multibeam image and morphology of the cross-shelf trough of Home Bay visualized with the QPS Fledermaus software.

Fig. S3. Correlation of cores 01-PC and 01-TWC (AMD0217-01 = 1Comp) based on density.

Fig. S4. RPI proxy vs. its normalizer for cores 77PC, 1Comp and 9CASQ.

Fig. S5. RPI proxy vs. its normalizer ARM and IRM for cores 77PC, 1Comp and 9CASQ.

Fig. S6. Multibeam image of the site of core 1Comp (AMD0217-01) sampled at the edge of a TMF visualized with the QPS Fledermaus software.